Cite as: Z. Lin *et al*., *Science* 10.1126/science.aaz4352 (2019).

TTC5 mediates autoregulation of tubulin via mRNA degradation

Zhewang Lin[1], Ivana Gasic[2]*, Viswanathan Chandrasekaran[1]*, Niklas Peters[1]†, Sichen Shao[3], Timothy J. Mitchison[2], Ramanujan S. Hegde[1]‡

[1]MRC Laboratory of Molecular Biology, Cambridge CB2 0QH, UK. [2]Department of Systems Biology, Blavatnik Institute, Harvard Medical School, Boston, MA 02115, USA. [3]Department of Cell Biology, Blavatnik Institute, Harvard Medical School, Boston, MA 02115, USA.

*These authors contributed equally to this work.

†Present address: Center for Molecular Biology of Heidelberg University (ZMBH), 69120 Heidelberg, Germany.

‡Corresponding author. Email: rhegde@mrc-lmb.cam.ac.uk

Tubulins play crucial roles in cell division, intracellular traffic, and cell shape. Tubulin concentration is autoregulated by feedback control of mRNA degradation via an unknown mechanism. Here, we identified tetratricopeptide protein 5 (TTC5) as a tubulin-specific ribosome-associating factor that triggers co-translational degradation of tubulin mRNAs in response to excess soluble tubulin. Structural analysis revealed that TTC5 binds near the ribosome exit tunnel and engages the N terminus of nascent tubulins. TTC5 mutants incapable of ribosome or nascent tubulin interaction abolished tubulin autoregulation and showed chromosome segregation defects during mitosis. Our findings show how a subset of mRNAs can be targeted for coordinated degradation by a specificity factor that recognizes the nascent polypeptides they encode.

Alpha and beta tubulins form obligate heterodimers (hereafter αβ-tubulin) that reversibly and dynamically polymerize into microtubules—cytoskeletal elements that regulate cell shape, drive mitosis, provide platforms for intracellular transport, and mediate cell movement (*1*). Microtubule dynamics, and the various processes that depend on it (*2*, *3*), are strongly influenced by the concentration of soluble (i.e., non-polymerized) αβ-tubulin (*4*). When cells detect an increase in soluble αβ-tubulin concentration, they trigger degradation of tubulin mRNAs via a process termed tubulin autoregulation (*5*–*7*).

Autoregulation requires translation, indicating that ribosome-engaged tubulin mRNAs are selectively targeted for degradation (*8*, *9*). Analysis of β-tubulin autoregulation in mammalian cells indicates a critical role for the first four residues (Met-Arg-Glu-Ile, or MREI) common to all β-tubulin isoforms (*10*, *11*). Because autoregulation is prevented by physical occlusion of the MREI motif (*12*), a factor is thought to engage this sequence on nascent tubulin to initiate degradation of the mRNA being translated.

We used a site-specific photo-crosslinking strategy (Fig. 1A and fig. S1) to detect cytosolic factors that specifically recognize the N-terminal autoregulatory motif (MREI) of nascent β-tubulin early during its translation. A ribosome nascent chain complex (RNC) displaying the first 94 amino acids of ^{35}S-methionine labeled human β-tubulin containing the UV-activated crosslinking amino acid *p*-benzoyl-l-phenylalanine (Bpa) was produced by in vitro translation in rabbit reticulocyte lysate. Irradiation of these RNCs with UV light generated nascent chain crosslinks to various proteins, only one of which was sensitive to mutation of residues 2, 3, and 4 of the MREI motif (Fig. 1B). This MREI-specific interaction partner was identified by quantitative mass spectrometry to be TTC5 (Fig. 1C), a highly conserved protein found widely across eukaryotes (fig. S2). TTC5 engaged the MREC motif at the N terminus of nascent α-tubulin comparably to the MREI motif on β-tubulin (Fig. 1D), consistent with position 4 being less critical than positions 2 or 3 (Fig. 1B) (*11*). Thus, TTC5 is a nascent polypeptide binding protein specific for the N-termini of α- and β-tubulins.

To understand how TTC5 engages its substrates on the ribosome, we purified nascent tubulin RNCs in complex with TTC5 (fig. S3) and determined its structure by single-particle electron cryomicroscopy (cryo-EM). The TTC5-RNC reconstruction (figs. S4 and S5) showed the ribosome with a peptidyl-tRNA, nascent β-tubulin polypeptide within the ribosome exit tunnel, and TTC5 bound at the mouth of the tunnel (Fig. 2A). The heterodimeric nascent polypeptide associated complex (NAC) was observed at its previously established binding site (*13*, *14*) opposite the exit tunnel

from TTC5 (see fig. S4). NAC is not specific to tubulin RNCs (*15*, *16*), does not contact TTC5 in the structure, and is not discussed further.

TTC5 was seen to make two contacts with the ribosome. The first contact involves three highly conserved lysine side chains in the oligonucleotide binding domain of TTC5 making electrostatic interactions with phosphates of the 28S rRNA backbone (Fig. 2B). The second contact involves ribosomal protein uL24 and buries ~ 500 Å^2 of TTC5 adjacent to a deep groove formed by the tetratricopeptide repeat domain of TTC5 (Fig. 2C). The groove faces the mouth of the exit tunnel and contains cryo-EM density that we assigned to the first eight amino acids of β-tubulin (fig. S5), consistent with photo-crosslinking results (fig. S6).

The structural model allowed us to deduce likely interactions between the MREI motif and conserved side chains lining the TTC5 groove (Fig. 2D). Depending on its orientation, the R2 side chain of nascent tubulin is within salt bridge distance of E259 and D225 of TTC5. E3 in nascent tubulin would likely interact with R147 in TTC5. The side chain of I4 faces a moderately hydrophobic surface that could accommodate a cysteine (as in α-tubulins) or possibly other amino acids consistent with earlier mutagenesis (*11*). Collectively, the structure shows how TTC5 binds near the ribosome exit tunnel with its peptide binding groove positioned to engage nascent tubulins shortly after they emerge from the ribosome.

Recombinant TTC5 containing Bpa at position 194 in the 'floor' of the peptide binding groove (Fig. 2D) efficiently crosslinked with MREI-containing nascent chains, weakly crosslinked with MREV-containing nascent chains, and did not crosslink with any other mutants (Fig. 3A). Analysis of RNC crosslinking with various TTC5 mutants (Fig. 3B) validated R147, D225, and E259 as key residues within the groove that likely interact with R2 and E3 of nascent tubulin (see Fig. 2D). Binding assays with purified TTC5 and synthetic peptides (Fig. 3C and fig. S7) verified these findings and additionally showed that M1 is critical for TTC5 binding and must strictly be at the N terminus. Thus, the structural analysis rationalizes all earlier β-tubulin mutagenesis studies on autoregulation requirement (*11*) and reveals the mechanistic basis of the exquisite specificity of autoregulation for α- and β-tubulins (*5*) that uniquely contain an MREI or MREC motif at the N terminus (*17*).

Mutating the ribosome-interacting residues K285 and K287 of TTC5 to glutamic acid (KK-EE) completely abolished β-tubulin RNC binding in the crosslinking assay (Fig. 3B) despite unperturbed binding of TTC5 to synthetic tubulin autoregulatory peptide in a thermal shift assay (Fig. 3C and fig. S7). Affinity purification of recombinant TTC5 from in vitro translation reactions of nascent β-tubulin RNCs showed that no ribosomes were recovered with either TTC5(KK-EE) or the peptide binding mutant TTC5(R147A), in contrast to wild-type TTC5 (Fig. 3D). Thus, the avidity of bi-partite binding to the ribosome and nascent tubulin imparts high affinity and specificity to the TTC5-RNC interaction.

CRISPR-mediated disruption of TTC5 expression in multiple cell lines completely abolished the decay of α- and β-tubulin mRNAs in response to acute microtubule destabilization (Fig. 4A and fig. S8). Pulse labeling with ^{35}S-methionine of wild type cells showed that of the major proteins visualized, tubulins were selectively reduced in their synthesis when cells are pre-treated with microtubule destabilizing agents (fig. S9). Selective reduction in tubulin protein synthesis was completely lost in TTC5 knockout cells, consistent with the failure to degrade tubulin mRNAs. Tubulin autoregulation, as judged by both mature- versus pre-mRNA levels (Fig. 4A) and rates of protein synthesis (fig. S9), could be restored to TTC5 knockout cells by re-expression of wild type TTC5 but not the peptide-binding mutant R147A or the ribosome-binding mutant KK-EE. Thus, TTC5 engagement of nascent tubulin at the ribosome is strictly required for tubulin mRNA degradation when cells initiate autoregulation. Access of TTC5 to the ribosome proved to be a regulated event.

The TTC5-RNC complex was found to be disrupted by a cytosolic factor whose activity was lost when cells were pre-treated with colchicine to initiate autoregulation (Fig. 4B and fig. S10). Loss of this inhibitory activity under autoregulation conditions was accompanied by increased capacity of TTC5 to engage tubulin RNCs as measured by recovery of tubulin mRNAs (Fig. 4C and fig. S11). These results indicate that cells ordinarily contain an inhibitory factor that prevents TTC5 engagement of tubulin RNCs. This TTC5 inhibitor is inactivated when cells perceive excess αβ-tubulin, freeing TTC5 to engage tubulin RNCs and trigger tubulin mRNA degradation. TTC5 access to RNCs only during autoregulation explains why normally growing TTC5 knockout cells did not show notably elevated tubulin mRNA and protein (fig. S12). Because overexpressed TTC5 in the rescue cell lines did not trigger tubulin mRNA degradation until cells perceive excess αβ-tubulin (fig. S12), it seems the inhibitor is not easily saturated. Future work will identify the inhibitor and its mechanism of regulation.

Chromosome alignment and segregation during mitosis are sensitive to altered microtubule dynamics (*18–21*), motivating us to monitor these parameters in cells impaired in tubulin autoregulation (Fig. 4D). TTC5 knockout HeLa cells showed ~6.5-fold higher rate of chromosome alignment errors in metaphase (Fig. 4E and fig. S13), ~2.4-fold higher rate of segregation errors during anaphase (Fig. 4E and fig. S13), and a subtle but highly reproducible increase of mitotic duration (fig. S14). These phenotypes in TTC5 knockout

cells were rescued by re-expression of wild type TTC5 but not the peptide binding or ribosome binding mutants of TTC5 (Fig. 4E and figs. S13 and S14). Although the specific basis of mitotic defects in TTC5 knockout cells remains to be determined, we can ascribe the phenotypes to autoregulation, and not another TTC5 function (*22*–*24*), because the effects were not rescued by two unrelated point mutants of TTC5 that perturb autoregulation by different mechanisms.

TTC5 represents a highly selective and regulated ribosome-associating factor that only engages the ~2-3% of a cell's ribosomes actively synthesizing α- and β-tubulins. By marking tubulin-translating ribosomes, TTC5 is ideally positioned to recruit yet unidentified downstream effectors to this site that trigger mRNA decay. More generally, the translating ribosome represents a platform from which to effect abundance control of key cellular proteins because translation initiation (*25*), elongation (*26*), polypeptide fate (*27*), and mRNA stability (*28*) can all be locally regulated from this site. Specificity for particular substrates would be imparted by recognition of the nascent protein emerging from the ribosome exit tunnel. Thus, cells may contain a family of substrate-specific ribosome-associating factors analogous to TTC5 that dynamically tune the abundance of key proteins such as histones (*29*) and chaperones (*30*). The methods and paradigm of co-translational abundance control established here should provide a framework for studying this mode of cellular regulation.

REFERENCES AND NOTES

1. G. Borisy, R. Heald, J. Howard, C. Janke, A. Musacchio, E. Nogales, Microtubules: 50 years on from the discovery of tubulin. *Nat. Rev. Mol. Cell Biol.* **17**, 322–328 (2016). doi:10.1038/nrm.2016.45 Medline
2. A. Desai, T. J. Mitchison, Microtubule polymerization dynamics. *Annu. Rev. Cell Dev. Biol.* **13**, 83–117 (1997). doi:10.1146/annurev.cellbio.13.1.83 Medline
3. G. J. Brouhard, L. M. Rice, Microtubule dynamics: An interplay of biochemistry and mechanics. *Nat. Rev. Mol. Cell Biol.* **19**, 451–463 (2018). doi:10.1038/s41580-018-0009-y Medline
4. R. A. Walker, E. T. O'Brien, N. K. Pryer, M. F. Soboeiro, W. A. Voter, H. P. Erickson, E. D. Salmon, Dynamic instability of individual microtubules analyzed by video light microscopy: Rate constants and transition frequencies. *J. Cell Biol.* **107**, 1437–1448 (1988). doi:10.1083/jcb.107.4.1437 Medline
5. I. Gasic, S. A. Boswell, T. J. Mitchison, Tubulin mRNA stability is sensitive to change in microtubule dynamics caused by multiple physiological and toxic cues. *PLOS Biol.* **17**, e3000225 (2019). doi:10.1371/journal.pbio.3000225 Medline
6. D. W. Cleveland, M. A. Lopata, P. Sherline, M. W. Kirschner, Unpolymerized tubulin modulates the level of tubulin mRNAs. *Cell* **25**, 537–546 (1981). doi:10.1016/0092-8674(81)90072-6 Medline
7. D. W. Cleveland, Autoregulated instability of tubulin mRNAs: A novel eukaryotic regulatory mechanism. *Trends Biochem. Sci.* **13**, 339–343 (1988). doi:10.1016/0968-0004(88)90103-X Medline
8. D. A. Gay, S. S. Sisodia, D. W. Cleveland, Autoregulatory control of β-tubulin mRNA stability is linked to translation elongation. *Proc. Natl. Acad. Sci. U.S.A.* **86**, 5763–5767 (1989). doi:10.1073/pnas.86.15.5763 Medline
9. J. S. Pachter, T. J. Yen, D. W. Cleveland, Autoregulation of tubulin expression is achieved through specific degradation of polysomal tubulin mRNAs. *Cell* **51**, 283–292 (1987). doi:10.1016/0092-8674(87)90155-3 Medline
10. T. J. Yen, P. S. Machlin, D. W. Cleveland, Autoregulated instability of β-tubulin mRNAs by recognition of the nascent amino terminus of β-tubulin. *Nature* **334**, 580–585 (1988). doi:10.1038/334580a0 Medline
11. C. J. Bachurski, N. G. Theodorakis, R. M. Coulson, D. W. Cleveland, An amino-terminal tetrapeptide specifies cotranslational degradation of β-tubulin but not α-tubulin mRNAs. *Mol. Cell. Biol.* **14**, 4076–4086 (1994). doi:10.1128/MCB.14.6.4076 Medline
12. N. G. Theodorakis, D. W. Cleveland, Physical evidence for cotranslational regulation of β-tubulin mRNA degradation. *Mol. Cell. Biol.* **12**, 791–799 (1992). doi:10.1128/MCB.12.2.791 Medline
13. M. Gamerdinger, K. Kobayashi, A. Wallisch, S. G. Kreft, C. Sailer, R. Schlömer, N. Sachs, A. Jomaa, F. Stengel, N. Ban, E. Deuerling, Early Scanning of Nascent Polypeptides inside the Ribosomal Tunnel by NAC. *Mol. Cell* **75**, 996–1006.e8 (2019). doi:10.1016/j.molcel.2019.06.030 Medline
14. R. D. Wegrzyn, D. Hofmann, F. Merz, R. Nikolay, T. Rauch, C. Graf, E. Deuerling, A conserved motif is prerequisite for the interaction of NAC with ribosomal protein L23 and nascent chains. *J. Biol. Chem.* **281**, 2847–2857 (2006). doi:10.1074/jbc.M511420200 Medline
15. B. Wiedmann, H. Sakai, T. A. Davis, M. Wiedmann, A protein complex required for signal-sequence-specific sorting and translocation. *Nature* **370**, 434–440 (1994). doi:10.1038/370434a0 Medline
16. M. Gamerdinger, M. A. Hanebuth, T. Frickey, E. Deuerling, The principle of antagonism ensures protein targeting specificity at the endoplasmic reticulum. *Science* **348**, 201–207 (2015). doi:10.1126/science.aaa5335 Medline
17. UniProt Consortium, UniProt: The universal protein knowledgebase. *Nucleic Acids Res.* **46**, 2699 (2018). doi:10.1093/nar/gky092 Medline
18. J. J. Vicente, L. Wordeman, The quantification and regulation of microtubule dynamics in the mitotic spindle. *Curr. Opin. Cell Biol.* **60**, 36–43 (2019). doi:10.1016/j.ceb.2019.03.017 Medline
19. S. Petry, Mechanisms of Mitotic Spindle Assembly. *Annu. Rev. Biochem.* **85**, 659–683 (2016). doi:10.1146/annurev-biochem-060815-014528 Medline
20. S. L. Prosser, L. Pelletier, Mitotic spindle assembly in animal cells: A fine balancing act. *Nat. Rev. Mol. Cell Biol.* **18**, 187–201 (2017). doi:10.1038/nrm.2016.162 Medline
21. S. L. Kline-Smith, C. E. Walczak, Mitotic spindle assembly and chromosome segregation: Refocusing on microtubule dynamics. *Mol. Cell* **15**, 317–327 (2004). doi:10.1016/j.molcel.2004.07.012 Medline
22. J. T. Lynch, T. D. D. Somerville, G. J. Spencer, X. Huang, T. C. P. Somervaille, TTC5 is required to prevent apoptosis of acute myeloid leukemia stem cells. *Cell Death Dis.* **4**, e573 (2013). doi:10.1038/cddis.2013.107 Medline
23. C. Demonacos, M. Krstic-Demonacos, N. B. La Thangue, A TPR motif cofactor contributes to p300 activity in the p53 response. *Mol. Cell* **8**, 71–84 (2001). doi:10.1016/S1097-2765(01)00277-5 Medline
24. X. Hu, R. D. Mullins, LC3 and STRAP regulate actin filament assembly by JMY during autophagosome formation. *J. Cell Biol.* **218**, 251–266 (2019). doi:10.1083/jcb.201802157 Medline
25. N. Sonenberg, A. G. Hinnebusch, Regulation of translation initiation in eukaryotes: Mechanisms and biological targets. *Cell* **136**, 731–745 (2009). doi:10.1016/j.cell.2009.01.042 Medline
26. J. C. Darnell, E. Klann, The translation of translational control by FMRP: Therapeutic targets for FXS. *Nat. Neurosci.* **16**, 1530–1536 (2013). doi:10.1038/nn.3379 Medline
27. O. Brandman, R. S. Hegde, Ribosome-associated protein quality control. *Nat. Struct. Mol. Biol.* **23**, 7–15 (2016). doi:10.1038/nsmb.3147 Medline
28. C. J. Shoemaker, R. Green, Translation drives mRNA quality control. *Nat. Struct. Mol. Biol.* **19**, 594–601 (2012). doi:10.1038/nsmb.2301 Medline
29. W. F. Marzluff, K. P. Koreski, Birth and Death of Histone mRNAs. *Trends Genet.*

33, 745–759 (2017). doi:10.1016/j.tig.2017.07.014 Medline

30. B. J. DiDomenico, G. E. Bugaisky, S. Lindquist, The heat shock response is self-regulated at both the transcriptional and posttranscriptional levels. *Cell* **31**, 593–603 (1982). doi:10.1016/0092-8674(82)90315-4 Medline
31. J. W. Chin, T. A. Cropp, J. C. Anderson, M. Mukherji, Z. Zhang, P. G. Schultz, An expanded eukaryotic genetic code. *Science* **301**, 964–967 (2003). doi:10.1126/science.1084772 Medline
32. K. Sakamoto, A. Hayashi, A. Sakamoto, D. Kiga, H. Nakayama, A. Soma, T. Kobayashi, M. Kitabatake, K. Takio, K. Saito, M. Shirouzu, I. Hirao, S. Yokoyama, Site-specific incorporation of an unnatural amino acid into proteins in mammalian cells. *Nucleic Acids Res.* **30**, 4692–4699 (2002). doi:10.1093/nar/gkf589 Medline
33. F. A. Ran, P. D. Hsu, J. Wright, V. Agarwala, D. A. Scott, F. Zhang, Genome engineering using the CRISPR-Cas9 system. *Nat. Protoc.* **8**, 2281–2308 (2013). doi:10.1038/nprot.2013.143 Medline
34. J. W. Chin, A. B. Martin, D. S. King, L. Wang, P. G. Schultz, Addition of a photocrosslinking amino acid to the genetic code of Escherichiacoli. *Proc. Natl. Acad. Sci. U.S.A.* **99**, 11020–11024 (2002). doi:10.1073/pnas.172226299 Medline
35. A. Sharma, M. Mariappan, S. Appathurai, R. S. Hegde, In vitro dissection of protein translocation into the mammalian endoplasmic reticulum. *Methods Mol. Biol.* **619**, 339–363 (2010). doi:10.1007/978-1-60327-412-8_20 Medline
36. Q. Feng, S. Shao, In vitro reconstitution of translational arrest pathways. *Methods* **137**, 20–36 (2018). doi:10.1016/j.ymeth.2017.12.018 Medline
37. K. J. Livak, T. D. Schmittgen, Analysis of relative gene expression data using real-time quantitative PCR and the 2(-Δ Δ C(T)) Method. *Methods* **25**, 402–408 (2001). doi:10.1006/meth.2001.1262 Medline
38. J. Zivanov, T. Nakane, B. O. Forsberg, D. Kimanius, W. J. H. Hagen, E. Lindahl, S. H. W. Scheres, New tools for automated high-resolution cryo-EM structure determination in RELION-3. *eLife* **7**, e42166 (2018). doi:10.7554/eLife.42166 Medline
39. S. Q. Zheng, E. Palovcak, J.-P. Armache, K. A. Verba, Y. Cheng, D. A. Agard, MotionCor2: Anisotropic correction of beam-induced motion for improved cryo-electron microscopy. *Nat. Methods* **14**, 331–332 (2017). doi:10.1038/nmeth.4193 Medline
40. A. Rohou, N. Grigorieff, CTFFIND4: Fast and accurate defocus estimation from electron micrographs. *J. Struct. Biol.* **192**, 216–221 (2015). doi:10.1016/j.jsb.2015.08.008 Medline
41. S. Shao, J. Murray, A. Brown, J. Taunton, V. Ramakrishnan, R. S. Hegde, Decoding Mammalian Ribosome-mRNA States by Translational GTPase Complexes. *Cell* **167**, 1229–1240.e15 (2016). doi:10.1016/j.cell.2016.10.046 Medline
42. C. J. Adams, A. C. W. Pike, S. Maniam, T. D. Sharpe, A. S. Coutts, S. Knapp, N. B. La Thangue, A. N. Bullock, The p53 cofactor Strap exhibits an unexpected TPR motif and oligonucleotide-binding (OB)-fold structure. *Proc. Natl. Acad. Sci. U.S.A.* **109**, 3778–3783 (2012). doi:10.1073/pnas.1113731109 Medline
43. A. Waterhouse, M. Bertoni, S. Bienert, G. Studer, G. Tauriello, R. Gumienny, F. T. Heer, T. A. P. de Beer, C. Rempfer, L. Bordoli, R. Lepore, T. Schwede, SWISS-MODEL: Homology modelling of protein structures and complexes. *Nucleic Acids Res.* **46**, W296–W303 (2018). doi:10.1093/nar/gky427 Medline
44. A. Brown, F. Long, R. A. Nicholls, J. Toots, P. Emsley, G. Murshudov, Tools for macromolecular model building and refinement into electron cryo-microscopy reconstructions. *Acta Crystallogr. D* **71**, 136–153 (2015). doi:10.1107/S1399004714021683 Medline
45. P. Emsley, B. Lohkamp, W. G. Scott, K. Cowtan, Features and development of Coot. *Acta Crystallogr. D* **66**, 486–501 (2010). doi:10.1107/S0907444910007493 Medline
46. L. Wang, W. Zhang, L. Wang, X. C. Zhang, X. Li, Z. Rao, Crystal structures of NAC domains of human nascent polypeptide-associated complex (NAC) and its αNAC subunit. *Protein Cell* **1**, 406–416 (2010). doi:10.1007/s13238-010-0049-3 Medline
47. V. B. Chen, W. B. Arendall 3rd, J. J. Headd, D. A. Keedy, R. M. Immormino, G. J. Kapral, L. W. Murray, J. S. Richardson, D. C. Richardson, MolProbity: All-atom structure validation for macromolecular crystallography. *Acta Crystallogr. D* **66**, 12–21 (2010). doi:10.1107/S0907444909042073 Medline
48. P. B. Rosenthal, R. Henderson, Optimal determination of particle orientation, absolute hand, and contrast loss in single-particle electron cryomicroscopy. *J. Mol. Biol.* **333**, 721–745 (2003). doi:10.1016/j.jmb.2003.07.013 Medline
49. E. F. Pettersen, T. D. Goddard, C. C. Huang, G. S. Couch, D. M. Greenblatt, E. C. Meng, T. E. Ferrin, UCSF Chimera—A visualization system for exploratory research and analysis. *J. Comput. Chem.* **25**, 1605–1612 (2004). doi:10.1002/jcc.20084 Medline

ACKNOWLEDGMENTS

We thank V. Ramakrishnan for support and advice; S.-Y. Peak-Chew and M. Skehel for mass spectrometry analysis; J. Grimmett and T. Darling for advice, data storage and high-performance computing; P. Emsley for advice; the MRC Laboratory of Molecular Biology EM Facility for microscopy support, sample preparation and data collection; Brian Raught and Wade Harper for Flp-In TRex HeLa cells; the Nikon Imaging Center at Harvard Medical School for help with light microscopy. **Funding:** This work was supported by the UK Medical Research Council (MC_UP_A022_1007 to R.S.H.), the US National Institutes of Health (NIH P50 107618 to T.J.M.), Harvard Medical School (S.S.) and Vallee Scholars Program (S.S.). Z.L. was supported by the Human Frontier Science Program postdoctoral fellowship. I.G. is a Merck Fellow of the Damon Runyon Cancer Research Foundation (DRG:2279-16). V.C. was supported by V. Ramakrishnan whose funding was from the MRC (MC_U105184332), the Wellcome Trust (WT096570 to V.R.), the Agouron Institute, and the Louis-Jeantet Foundation. **Author contributions:** ZL discovered TTC5 and performed all biochemical analyses. IG and SS generated and validated HeLa cell lines. IG designed and performed phenotypic analysis of mitosis. VC performed structural analysis of the TTC5-ribosome complex. NP set up and characterized the in vitro photo-crosslinking system. SS, TJM, and RSH supervised different aspects of the project. RSH and ZL conceived the project, oversaw its implementation, and wrote the manuscript. All authors contributed to manuscript editing. **Competing interests:** The authors declare no competing interests. **Data and materials availability:** The cryo-EM map has been deposited to the EMDB (EMD-10380) and atomic coordinates have been deposited to the Protein Data Bank (PDB 6T59). All other data are available in the manuscript or the supplementary material.

SUPPLEMENTARY MATERIALS

science.sciencemag.org/cgi/content/full/science.aaz4352/DC1
Materials and Methods
Figs. S1 to S15
Table S1
References (*31*–*49*)

9 September 2019; accepted 31 October 2019
Published online 14 November 2019
10.1126/science.aaz4352

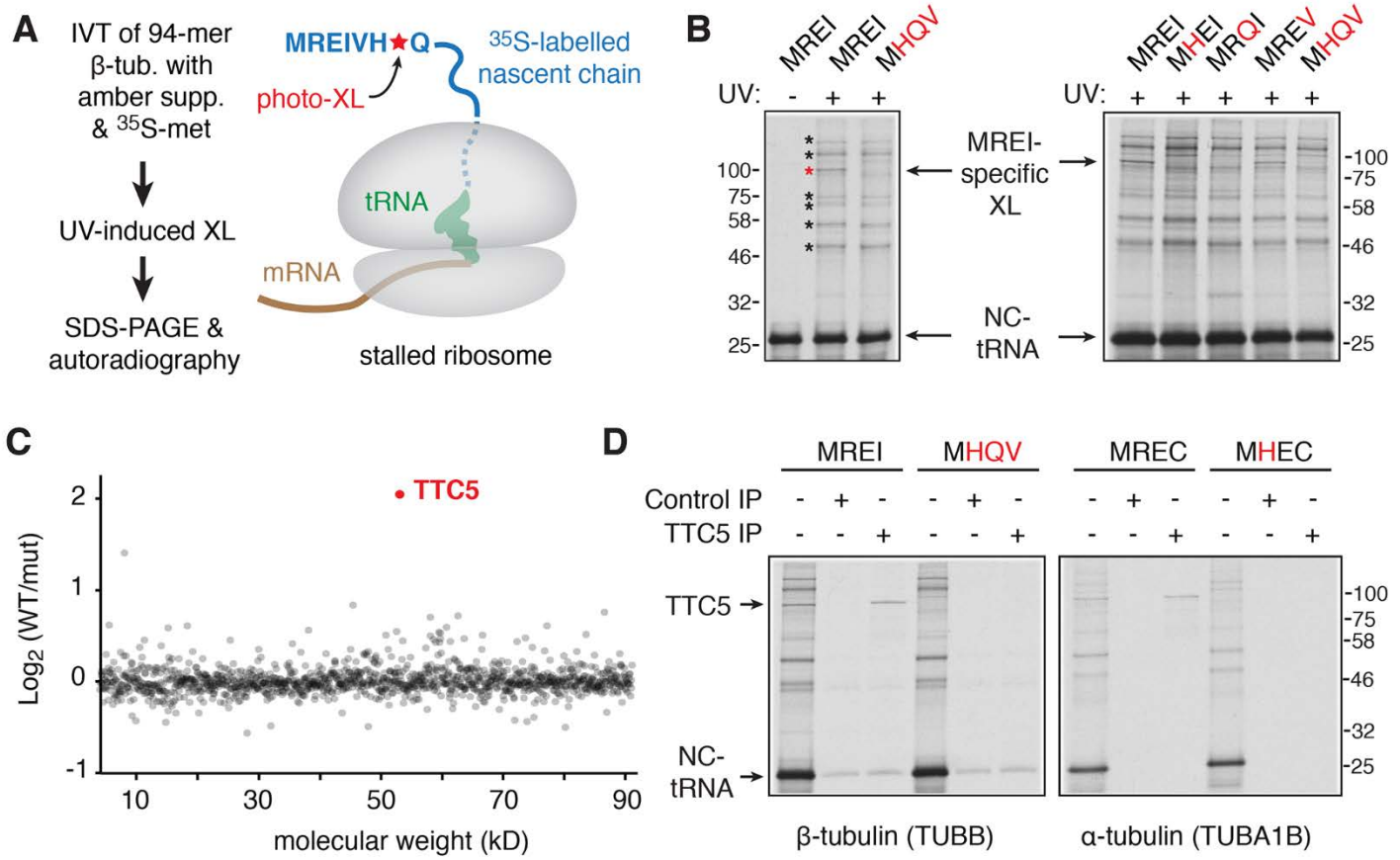

Fig. 1. TTC5 interacts with the N-termini of nascent tubulins. (**A**) Experimental strategy to detect interaction partners close to the N terminus of nascent tubulin. The UV-activated crosslinking amino acid *p*-benzoyl-l-phenylalanine (Bpa) is introduced site-specifically at position 7 using amber suppression (see fig. S1). (**B**) Photo-crosslinking analysis of ^{35}S-labeled 94-amino acid long ribosome-nascent chain complexes (RNCs) of human β-tubulin and mutants (indicated in red) in the N-terminal MREI motif. The positions of non-crosslinked tRNA-associated nascent chain (NC-tRNA) and a crosslinking partner specific to wild type tubulin (red asterisk) are indicated. Other nascent chain crosslinks agnostic to the MREI motif are indicated by black asterisks. (**C**) Quantitative mass spectrometry of proteins co-purified with wild type (WT) versus MHQV mutant (mut) β-tubulin RNCs plotted by molecular weight. (**D**) Photo-crosslinking and immunopreciptation (IP) analysis of ^{35}S-labeled 94-amino acid long RNCs of α- or β-tubulin compared to the indicated mutants.

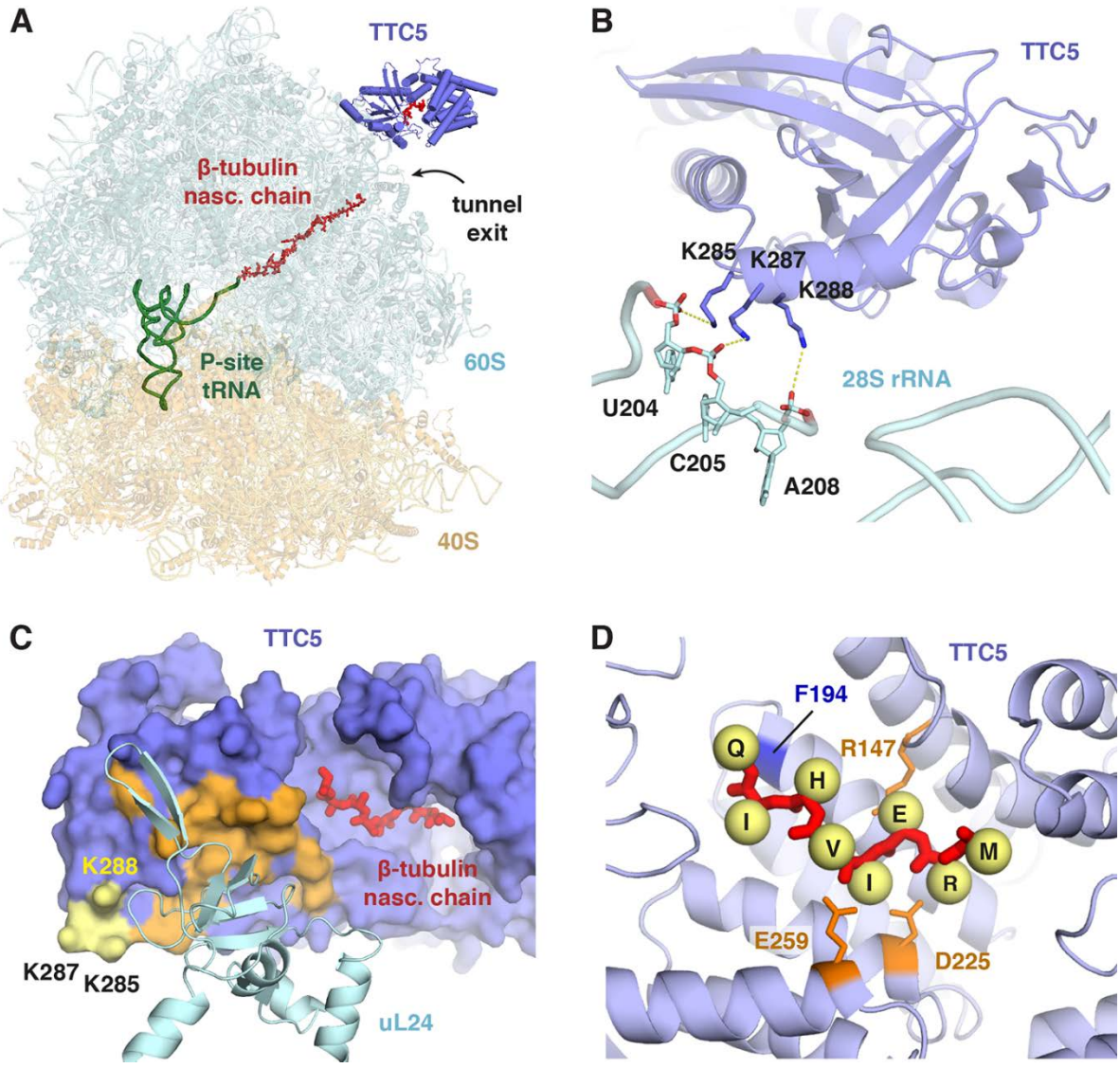

Fig. 2. Mechanism of ribosome-nascent chain engagement by TTC5. (**A**) Overview of the cryo-EM derived structure of the complex between TTC5 and a ribosome containing the first 64 amino acids of β-tubulin. (**B**) Close-up view of the TTC5 interaction with 28S rRNA. Three conserved lysine residues in TTC5 within electrostatic interaction distance of the rRNA backbone are indicated. (**C**) The surface of TTC5 that interacts with ribosomal protein uL24 is indicated in orange. The 28S-interacting residues from (B) are shown in yellow. The N-terminal 8 amino acids of the β-tubulin nascent chain is shown in red within its binding groove of TTC5. (**D**) Close-up view of the N-terminal 8 amino acids of nascent β-tubulin (MREIVHIQ) within TTC5. Yellow spheres denote C-β atoms for the indicated side chains (not modeled). R147 is within salt-bridge distance of E3, and D225 and E259 are within salt-bridge distance of R2. F194 on the 'floor' of the binding groove, shown in Fig. 3A to crosslink with nascent β-tubulin, is indicated.

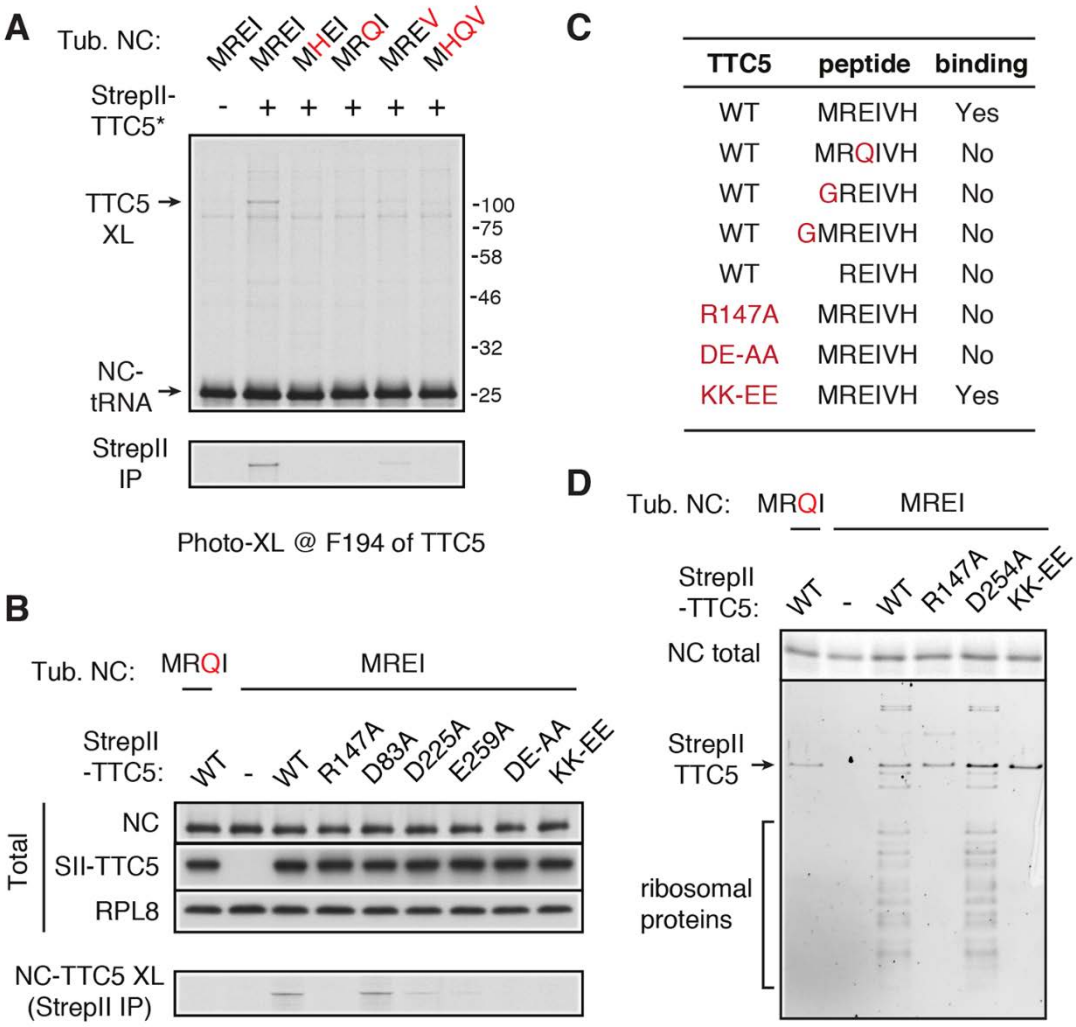

Fig. 3. Avidity-based RNC binding imparts specificity to TTC5. (**A**) Photo-crosslinking analysis of ^{35}S-labeled 94-amino acid long ribosome-nascent chain complexes (RNCs) of human β-tubulin and N-terminal mutants (indicated in red) with recombinant StrepII-tagged TTC5 containing the photo-crosslinking residue Bpa at position F194. The nascent chain crosslink to TTC5 is indicated (TTC5-XL) and verified by pulldown via the StrepII tag (bottom panel). (**B**) Photo-crosslinking analysis using ^{35}S-labeled 64-amino acid long ribosome-nascent chain complexes (RNCs) of human β-tubulin or the N-terminal MRQI mutant. Wild type or mutant recombinant StrepII-tagged TTC5 was included in the assay as indicated. The photo-crosslinking residue Bpa is at position 7 of the β-tubulin nascent chain. An aliquot of the total translation reaction was analyzed to verify equal levels of nascent chain (NC) synthesis by autoradiography and equal levels of recombinant TTC5 (SII-TTC5) by immunoblotting for the StrepII tag. The remainder was UV irradiated and TTC5 crosslinks were recovered via the StrepII tag and visualized by autoradiography (bottom panel). (**C**) Summary of interaction analysis between the indicated recombinant TTC5 proteins and the indicated synthetic peptides in a thermal shift denaturation assay (see fig. S7). (**D**) Wild type or mutant StrepII-tagged TTC5 was included during in vitro translation of wild type or mutant 64-mer β-tubulin RNCs as indicated. Equal translation of ^{35}S-labeled nascent chain synthesis was verified (NC total). The remainder of each translation was affinity purified via the StrepII tag and analyzed by staining of total proteins (bottom panel).

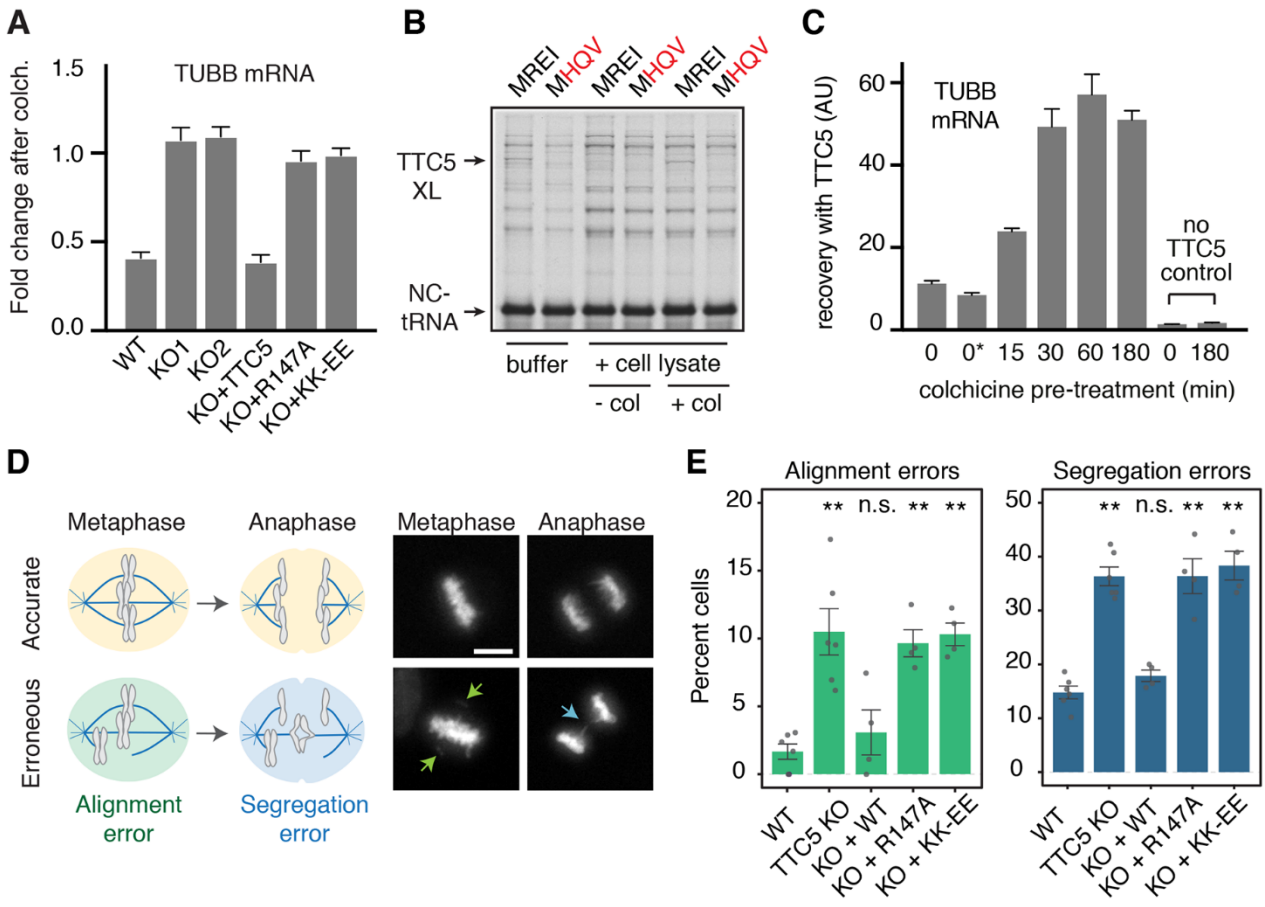

Fig. 4. TTC5 is required for tubulin autoregulation and accurate mitosis. (**A**) The indicated HEK293 cell lines were either left untreated or treated for 3 hours with colchicine. The relative amounts of the indicated mRNAs or pre-mRNAs were quantified by RT-qPCR and normalized to a control ribosomal RNA. Plotted is the mean ± SD from three replicates. Similar results are seen in HeLa cells and with different microtubule destabilizing agents (fig. S8). (**B**) Pre-formed RNC-TTC5 complexes (see fig. S10) were mixed with buffer or cytosol from TTC5 knockout cells that had been pre-treated (+col) or not (-col) with colchicine for 3 hours. All samples were subjected to UV crosslinking to monitor the nascent chain interactions. The positions of the non-crosslinked tRNA linked nascent chain (NC-tRNA) and TTC5 crosslink (TTC5-XL) are indicated. (**C**) TTC5-knockout HEK293 cells were pre-treated for the indicated times with colchicine and used to prepare lysates. One of the control samples included colchicine added after cell lysis (indicated as 0*). The products recovered by binding to recombinant TTC5 were analyzed for β-tubulin mRNA by quantitative RT-PCR. The relative recoveries are plotted (mean ± SD from three replicates). Similar results were seen for α-tubulin and when nocodazole was used instead of colchicine to trigger autoregulation (fig. S11). (**D**) Diagram (left) and examples (right) of accurate (top) and erroneous (bottom) chromosome alignment and segregation visualized with SirDNA dye during mitosis in HeLa cell lines (see fig. S13). Scale bar = 5 μm. (**E**) Quantification of errors in chromosome alignment and segregation in the indicated HeLa cell lines. Plotted is mean ± SEM from 4-6 independent biological replicates (dots) with 200-400 analyzed cells per replicate. Not significant (n.s.) and $p < 0.001$ (**) in paired Student's *t* tests are indicated.

science.sciencemag.org/cgi/content/full/science.aaz4352/DC1

Supplementary Materials for

TTC5 mediates autoregulation of tubulin via mRNA degradation

Zhewang Lin, Ivana Gasic, Viswanathan Chandrasekaran, Niklas Peters, Sichen Shao, Timothy J. Mitchison, Ramanujan S. Hegde*

*Corresponding author. Email: rhegde@mrc-lmb.cam.ac.uk

Published 14 November 2019 on *Science* First Release
DOI: 10.1126/science.aaz4352

This PDF file includes:

Materials and Methods

Plasmids and reagents

Tubulin constructs (human TUBB and TUBA1B) for in vitro translation in reticulocyte lysate (RRL) were cloned into pCDNA3.1. Constructs used for the expression and purification of WT or mutants 6XHis-StrepII-TTC5 human recombinant proteins were in the pET28a vector. Mutant *E.coli* tyrosyl-tRNA synthetase for incorporation of Bpa (*31*) was expressed and purified from pET21 vector. B*acillus stearothermophilus* suppressor $tRNA^{Tyr}$ sequence (*32*) carrying 5' T7 promoter sequence and a 3' BSTN1 restriction site was cloned into pRSET. For generation of stable cell lines, human TTC5 WT or mutants were sub-cloned into the pcDNA 5/FRT/TO vector. CRISPR Cas9 mediated TTC5 knockout used the following guide RNAs in the pX459 plasmid:

Exon 2 guide: (5'-TCATACTTTTTAGGAACTCG-3')
Exon 3 guide: (5'- TCAGCCTTAGGGCTATAGTC -3')
Exon 4 guide: (5'- GCTGACGAAGCACCATTGAC -3')

Cell Cultures

Flp-In TRex 293 cells (Invitrogen) were maintained in DMEM supplemented with 10% fetal calf serum and 2 mM L-glutamine. Flp-In TRex HeLa cells (from Brian Raught, University of Toronto) were maintained in DMEM supplemented with 10% fetal calf serum. CRISPR-Cas9 mediated gene disruption was performed in the Flp-In TRex 293 and HeLa cells as described (33). Briefly, cells were transiently transfected with the pX459 plasmid encoding the gRNAs targeting TTC5. 24 hours after transfection, 2 μg/ml puromycin was added for selection. 3 days after transfection, cells were trypsinized and re-plated in 96-well plates at a density of 0.5 cells per well to obtain single cell clones. Successful knockout clones were verified by anti-TTC5 western blot (TTC5 Polyclonal Antibody, Epigentek A66330 and Novus Biologicals NBP1-76636) and genotyping via PCR amplification of the modified region (see fig. S15 for an example). TTC5 rescue cell lines with stable expression of N-terminal FLAG-tagged WT or mutant TTC5 were generated from the TTC5-knockout cells using the Flp-In system (Invitrogen) according to manufacturer's protocol. Expression of transgene was induced with doxycycline (1 μg/mL) for 24-48h. Colchicine (10 μM), nocodazole (10 μM), and combretastatin A4 (1 μM) treatments were performed in standard media for the indicated time.

Live cell imaging and data analysis

Flp-In TRex HeLa of the genotypes indicated in the figure legends were plated in 8-well Lab Tek II Chamber 1.5 German coverglass dishes (Thermo Fisher, 155409) in regular growth medium, and incubated for 6 hours. Medium was then changed to DMEM with HEPES and without phenol-red (Thermo Fisher, 21063045) supplemented with 10% fetal calf serum, 10 ng/ml doxycycline and 200 nM SiR-DNA (Cytoskeleton, CY-SC007). Cells were incubated for 24 hours prior to imaging. Time lapse images were acquired using widefield inverted Nikon Ti fluorescence microscope (Nikon), equipped with Hamamatsu ORCA-ER cooled CCD camera (Hamamatsu), Proscan III motorized stage and shutters (Prior Scientific), SOLA light engine for fluorescence illumination (Lumencor), perfect focus system, and an incubation chamber with 37 C and 5% CO_2

cage (OkoLab). Three-dimensional Images at multiple stage positions were acquired in steps of 2 µm, every 7 minutes for 10 hours using MetaMorph (Molecular Devices) and 20x PlanApo objective (NA 0.75, Nikon). Single images were reconstructed into 3D movies using Fiji (ImageJ). Maximum intensity projections of representative examples of mitoses were prepared in Fiji and exported either as movies or still images. Analysis of mitotic cells was performed using 3D reconstructions in Fiji. The parameters scored (based on SiR-DNA signal) were time from nuclear envelope breakdown (NEB) to telophase (two-cell stage), occurrence of unaligned chromosomes in metaphase, and chromosome segregation errors in anaphase. Data analyses were documented using Excel and processed and plotted using R. Statistical analyses were performed in R and Excel.

Recombinant protein and tRNA purification

WT and mutant 6XHis-StrepII tagged TTC5 were purified from E. coli (BL21) cells. Briefly, cells were transformed with the pET28a plasmid encoding the WT or mutant TTC5 and grown at 37 °C in LB containing 50 µg/mL kanamycin. Induction was with 0.2 mM IPTG at an A600 of 0.6 at 16 °C overnight. For Bpa incorporation at position 194 in TTC5 protein, the cells were co-transformed with the pET28a plasmid encoding the amber mutant TTC5 and the pEVOL-pBpF plasmid [addgene #31190; (*34*)]. Cells were grown at 37 °C in LB containing 50 µg/mL kanamycin and 25 µg/mL chloramphenicol and induced with 0.2% L-arabinose at an A600 of 0.3 for 30 min followed by a second induction with 0.2 mM IPTG at an A600 of ~0.6 at 16 °C overnight. Bacterial lysate was prepared by sonication in 30 mL cold lysis buffer (500 mM NaCl, 20 mM imidazole, 1 mM phenylmethylsulfonyl fluoride, 1 mM TCEP and 50 mM HEPES, pH 7.4) per L of cells. Clarified bacterial lysates from a 1 L culture were bound to 1 mL column of Ni-NTA (Qiagen) by gravity flow. Columns were washed with ~10 column volumes of lysis buffer and eluted with 250 mM imidazole in lysis buffer. The eluate was then bound to a 200 µL column of Streptactin Sepharose® High Performance (GE Healthcare, 28-9355-99). After extensive washing with 500 mM NaCl, 1 mM TECP and 20 mM Hepes, pH 7.4, the bound TTC5 protein was eluted with 500 µL washing buffer containing 25 mM biotin and dialyzed twice against dialysis buffer (500 mM NaCl, 1 mM TECP and 20 mM Hepes, pH 7.4). *E.coli* Bpa tyrosyl-tRNA synthetase was purified via the C-terminal His tag on a 5 mL HiTrap Ni-NTA column (GE), desalted by a gel filtration column on FPLC and concentrated by Amicon Ultra centrifugal filter (Millipore, Z717185-8EA). *B. stearothermophilus* $tRNA^{Tyr}$, was synthesized by in vitro transcription. The pRSET-based construct was digested with BSTN1, yielding a DNA fragment containing the exact $tRNA^{Tyr}$ sequence under a T7 promoter. 5 mL transcription reaction was carried out with 1.2 mg DNA template, 1 mM spermidine, 5 mM DTT, 0.1% Triton, 5 mM NTPs, 25 µM $MgCl^2$, 20 µg/mL E. *coli* pyrophosphatase, 20 µg/mL T7 polymerase and 125 U Recombinant RNasin (Promega) for 4 hours at 37 °C. The reaction product was digested with Turbo DNase (Ambion) and extracted by acid phenol chloroform extraction to yield purified tRNA.

Western blot analysis

Samples were analyzed using 12% Tris-Tricine based gels, and transferred to 0.2 mm nitrocellulose membrane (Biorad). Primary antibody incubations were either for 1h at room temperature or 4 °C overnight. Detection used HRP-conjugated secondary

antibodies and SuperSignal West Pico Chemiluminescent substrate (Thermo Fisher), or DyLight conjugated antibodies (Thermo Fisher) and Odyssey Infra-Red Imaging System (LI-COR). Expression of N-FLAG WT or mutant TTC5 in rescue cell lines was detected by anti-FLAG M2-HRP (Sigma A8592), or monoclonal anti-FLAG M2 (Sigma, F3165). RPL8 protein was detected by anti-RPL8 antibody (abcam, ab155136), and tubulin proteins by anti-α-tubulin antibody (Sigma, T6199) or anti-β-tubulin antibody (Cell Signaling Technologies, 2128).

In vitro transcription and translation

All in vitro transcription of tubulin constructs utilized PCR product as template. The 5' primer contains the SP6 promoter sequence and anneals to the CMV promoter of pCDNA3.1. The 3' primers anneal at codon 54-60 or 84-90 of nascent tubulin and contain extra sequence encoding MKLV to generate 64-mer or 94-mer constructs respectively. Transcription reactions were carried out with SP6 polymerase for 1 hour at 37 °C. Transcription reactions were directly used for in vitro translation in a homemade rabbit reticulocyte lysate (RRL)-based translation system as previously described (35, 36).For incorporation of Bpa by amber suppression, 5 μM B. Stearothermophilus tRNATyr, 0.25 μM Bpa tyrosyl-tRNA synthetase, and 0.1 mM Bpa were included in the translation reaction. Where indicated in the figure legends, WT or mutant 6XHis-strepII-tagged TTC5s were included in the translation reactions. Translation reactions were at 32 °C for 20 min unless stated otherwise. For analysis of total translation level of nascent chains, a 1 μL aliquot of the translation reaction was mixed with protein sample buffer and analyzed by SDS-PAGE gel electrophoresis and autoradiography.

TTC5-RNC UV crosslinking analysis

Crosslinking was performed on isolated RNCs stalled after synthesis of a defined number of amino acids. Stalling was achieved by using a transcript truncated within the coding region at the desired codon (*35*, *36*). When ribosomes reach the end of such a mRNA, they stall. To isolate the stalled RNCs, 50 μL translation reactions were rapidly cooled on ice and layered on a 200 μL sucrose cushion in physiological salt buffer (PSB: 50 mM Hepes, pH 7.4, 100 mM KAc, 2 mM $MgCl_2$). Centrifugation was in a TLA 120.1 rotor (Beckman) at 100,000 rpm for 1 hour at 4 °C. The ribosome pellets were resuspended in 20 μL PSB on ice. The isolated RNCs were placed on ice ~10 cm away from a UVP B-100 series lamp (UVP LLC) for 10 minutes. For analysis of total crosslinking products, 2.5 μL of the reactions were mixed directly with protein sample buffer for SDS-PAGE gel electrophoresis and analyzed by autoradiography. For immunoprecipitation of tubulin nascent chain and endogenous TTC5 crosslinking product, 20 μL of the crosslinking reactions were adjusted to 1% SDS, denatured by heating at 95 °C for 1 min, diluted 10 fold with 180 μL IP buffer (100 mM NaCl, 50 mM Hepes, pH 7.4, 1% Triton X-100) and incubated with 1μg of TTC5 antibody and 5μL of protein A agarose at 4 °C for 2 hours. Beads were washed three times with 400 μL IP buffer and eluted with protein sample buffer for SDS-PAGE gel electrophoresis and autoradiography. For TTC5-RNC UV crosslinking in the presence of cytosolic lysates, isolated RNCs were pre-incubated with 2 mg/mL lysates for 5 min on ice before UV crosslinking. Note that cell lysates were prepared on ice. At this temperature, nearly all microtubules depolymerize during lysate preparation, and the minor population that does not is removed by centrifugation. Thus,

the cell lysates do not contain intact microtubules, and the soluble tubulin content of lysates prepared from untreated and colchicine/nocodazole treated cells are the same. For this reason, the inhibitor detected in Fig. 4B is not likely to be polymerized tubulin.

Quantitative mass spectrometry analysis of RNC associated proteins

Total ribosomes and associated proteins from translation reactions of WT or mutant nascent β-tubulin 64-mer were isolated by centrifugation as described above. The experiment was performed in duplicate. Quantitative mass spectrometry was performed by in-solution digestion of samples, followed by tandem mass tag labelling (Thermo Fisher Scientific cat. #90110). Protein samples in solution were reduced with 5 mM DTT at 56 °C for 30 min and alkylated with 10 mM iodoacetamide for 30 min in the dark at 22 °C. The alkylation reaction was quenched by the addition of DTT and the samples were digested with trypsin (Promega, 0.5 µg) overnight at 37 °C. The peptide mixtures were then desalted using home-made C18 (3M Empore) stage tip filled with 0.5mg of poros R3 (Applied Biosystems) resin. Bound peptides were eluted sequentially with 30%, 50% and 80% acetonitrile in 0.1%TFA and lyophilized. Dried peptide mixtures from each condition were resuspended in 20 µL of 7% acetonitrile, 200 mM triethyl ammonium bicarbonate. For TMT labelling, 0.8 mg of TMT reagents (Thermo Fisher Scientific) were reconstituted in 41 µL anhydrous acetonitrile. 10 µL of TMT was added to each peptide mixture and incubated for 1 hour at room temperature. The labelling reactions were terminated by incubation with 2.5 µL 5% hydroxylamine for 15 min, and labelled samples were subsequently pooled. The acetonitrile was evaporated using a Speed Vac, desalted and then fractionated with home-made C18 (3M Empore) stage tip using 10 mM ammonium bicarbonate and acetonitrile gradients. Eluted fractions were partially dried down using a Speed Vac and subjected to LC-MSMS. Liquid chromatography was performed on a fully automated Ultimate 3000 RSLC nano System (Thermo Scientific) fitted with a 100 μm × 2 cm PepMap100 C18 nano trap column and a 75 µm × 25 cm reverse phase C18 nano column (Aclaim PepMap, Thermo Scientific). Samples were separated using a binary gradient consisting of buffer A (2% acetonitrile, 0.1% formic acid) and buffer B (80% acetonitrile, 0.1% formic acid). Peptides were eluted at 300 nL/min with an acetonitrile gradient. The HPLC system was coupled to a Q Exactive Plus hybrid quardrupole-Orbitrap mass spectrometer (Thermo Fisher Scientific) equipped with a nanospray ion source. The acquired MSMS raw files were processed using Proteome Discoverer (version 2.1, Thermo Scientific). MSMS spectra were searched against mammals, UniProt Fasta database using Mascot (version 2.4, Matrix Science) search engine.

Affinity purification of TTC5-RNC complex

For analytical experiments, 20 µL translation reactions of nascent β-tubulin 64-mer containing 250 nM WT or mutant 6XHis-StrepII tagged TTC5s were carried out. The reactions were diluted 10 fold with 180 µL PSB and incubated with 5 μL streptactin sepharose at 4 °C for 2 hours. Beads were washed four times with 400 µL PSB and eluted with 20uL 25 mM biotin in PSB at 4 °C for 30 min. Eluates were mixed with protein sample buffer for SDS-PAGE gel electrophoresis and analyzed with sypro ruby protein gel stain (Thermo Fisher Scientific cat. S12000). For preparative scale purification of the TTC5-RNC complex for cryo-EM analysis, a 2 mL translation reaction containing 250

nM WT 6XHis-StrepII tagged TTC5 and non-radioactive methionine (40 μM) was incubated at 32 °C for 30 min. The reaction was cooled on ice and incubated with 20 μL streptactin sepharose at 4 °C for 2 hours. Beads were washed four times with 400 μL PSB and eluted with 40 μL 25 mM biotin in PSB at 4 °C for 30 min.

Thermal shift assay

The binding of synthetic peptides to recombinant TTC5 proteins were analyzed by thermal melting temperature using the nano-Differential Scanning Fluorimetry (NanoDSF, 2bind). 4 µM of WT or mutant TTC5 proteins were mixed with the indicated synthetic peptides (custom peptide synthesis by Genescript) in 100 mM HEPES pH 7.4, 250 mM NaCl. The capillaries were filled with 10 μL samples and placed on the sample holder. A temperature gradient of 2 °C·min^{-1} from 25 to 95 °C was applied and the intrinsic protein fluorescence at 330 and 350 nm was recorded. The first derivative of the 350 nm and 330 nm fluorescence ratio was plotted. The maximum of the peak corresponds to the melting temperature of the protein (inflection point of the ratio curve).

RT-qPCR for mRNA

HEK293 cells were grown to 70-80% confluency in 35 mm dish and treated with DMSO (control), colchicine (10 µM) or nocodazole (10 µM) for 3 hours. Cells were harvested and total RNA isolated using the RNeasy mini kit (QIAGEN, 74104) as per the manufacturers protocol. On column DNase digestion was performed. 500 ng of total RNA was used to generate cDNA using the iScript cDNA synthesis kit (BioRad). Samples were then kept on ice while they were made up to a volume of 100 µL with nuclease-free water. Small quantities of all samples were pooled and subsequently serially diluted to make standards. Samples were diluted ten-fold to ensure their values fell within the standard curve. RT-qPCR was carried out using a ViiA 7 Real-Time PCR System (Thermo Fisher Scientific) and KAPA SYBR Fast qPCR reagents (KAPA Biosystems) as per manufacturers instructions. The primer sequences used are listed below. All pairs of primers were annealed at 60 °C, and a melt curve performed. PCR products were verified by sequencing. Data was then analyzed using the Quantstudio Real-time PCR software v1.3. Values were normalized to the standard curve and against RPLP1 or GAPDH. Experiments include three biological replicates.

HeLa cells were grown to 70-80% confluency in 100 mm dishes and treated with DMSO (control) or combretastatin A4 (1 µM) 4 hours. Cells were harvested and total RNA isolated using the PureLink RNA Mini Kit (Invitrogen, Thermo Fisher, 12183018A) as per the manufacturers protocol. On column DNase digestion was performed using PureLink DNase Set (Thermo Fisher, 12185010) as per manufacturer's instructions. 500 ng of total RNA was used to generate cDNA using the SuperScript IV (Invitrogen, 18091050) and random hexamer primers, and following manufacturer's protocol. Samples were serially diluted to make standards. RT-qPCR was carried out using 5 ng of cDNA and 2x PowerUp SYBR Green master mix (Thermo Fisher, A25776) on a BioRad thermocycler (BioRad), as per manufacturer's instructions. Previously described and validated primers were used (*5*).All pairs of primers were annealed at 60 °C, and a melt curves performed. Data analysis was performed using the ddCt method (*37*).All data were normalized to reference genes RPL19 or GAPDH, and to DMSO

treated controls. Experiments include three biological replicates. Processing, statistical analysis, and data plotting were performed in R.

RT-qPCR primers used in this study

Target gene	Description	Sequence
TUBA1B	mRNA_Forward	5'-AATTCGCAAGCTGGCTGA-3'
	mRNA_Reverse	5'-CGACAGATGTCATAGATGGCC-3'
	pre-mRNA_Forward	5'-CACAGTCATTGGTGAGTTGAC-3'
	pre-mRNA_Reverse	5'-GTGCTTACCAGCTTGCGAAT-3'
TUBA1A	mRNA_Forward	5'-CCACAGTCATTGATGAAGTTCG-3'
	mRNA_Reverse	5'-GCTGTGGAAAACCAAGAAGC-3'
	pre-mRNA_Forward	5'-GCAGCATTTGTAGCAGGTGA-3'
	pre-mRNA_Reverse	5'-GCATTGCCAATCTGGACAC-3'
TUBB	mRNA_Forward	5'-GAAGCCACAGGTGGCAAATA-3'
	mRNA_Reverse	5'-CGTACCACATCCAGGACAGA-3'
	pre-mRNA_Forward	5'-CTGGACCGCATCTCTGTGTA-3'
	pre-mRNA_Reverse	5'-GGTTCACGAAAGGGACAAAA-3'
GAPDH	mRNA_Forward	5'-AGCTCATTTCCTGGTATGACA-3'
	mRNA_Reverse	5'-AGGGGAGATTCAGTGTGGTG-3'
RPLP1	mRNA_Forward	5'-CTCACTTCATCCGGCGACTAG-3'
	mRNA_Reverse	5'-GCAGAATGAGGGCCGAGTAG-3'
RPL19	mRNA_Forward	5'-ATCGCCACATGTATCACAGC-3'
	mRNA_Reverse	5'-TTGGTCTCTTCCTCCTTGGAT-3'

Recombinant TTC5 pulldown assays of cell lysates

TTC5-knockout cells were grown to 70-80% confluency in 145 mm dish and treated with DMSO control, colchicine (10 μM) or nocodazole (10 μM) for the times indicated in the figure legends. For preparation of cytosolic cell lysates, cells were pelleted by centrifugation at 500g for 5 min and lysed with lysis buffer [100 mM KAc, 5 mM $MgAc_2$, 1 mM DTT, 100 μg/mL digitonin, 1X EDTA-free protease inhibitor cocktail (Roche) and 50 mM HEPES, pH 7.4] for 10 min on ice. Lysates were cleared by centrifugation at 20,000 g for 5 min at 4 °C. Lysate concentrations were determined by Pierce BCA assay kit (Thermo Fisher). Note that on ice, nearly all microtubules depolymerize. Thus, the cell lysates do not contain microtubules, and the soluble tubulin content of lysates prepared from untreated and colchicine/nocodazole treated cells are the same. An aliquot of the lysates was used for total cytosolic RNA extraction and analyzed for tubulin mRNA content by RT-qPCR as described above. Another aliquot of each lysates was incubated with 500 nM recombinant TTC5 for 2 min on ice and incubated with 10 μL streptactin sepharose for 2 hours at 4 °C to recover TTC5 and all bound components. Control samples omitted recombinant TTC5. Beads were washed three times with 400 μL PSB and eluted with 50 μL 25 mM biotin in PSB at 4 °C for 30 min. The eluted products were used to isolate RNA using the RNeasy mini kit and used to generated cDNA using the iScript cDNA synthesis kit. Tubulin mRNAs in the elution were analyzed via RT-qPCR as described above.

Pulse labelling of protein synthesis

Cells were grown to 70-80% confluency in 35mm dish prior to labelling. Cells were washed two times with 2mL warm 1XPBS and starved for 30 min at 37 °C in media

lacking methionine. Labelling was initiated by addition of ^{35}S-methionine to a final concentration of 100 µCi per ml and incubated at 37 °C for 30 min. After the labeling period, cells were pelleted by centrifugation at 500 g for 2 min at 4 °C and lysed with 200µL lysis buffer [100 mM KAc, 5 mM $MgAc_2$, 1 mM DTT, 100 μg/mL digitonin, 1X EDTA-free protease inhibitor cocktail (Roche) and 50 mM HEPES, pH 7.4] for 10 min on ice. 3 μL of cleared lysate was mixed with protein sample buffer for SDS-PAGE to detect total translation product via autoradiography. For immunoprecipitation of α- and β-tubulin, 50 μL of the lysate was denatured by heating at 95 °C for 1 min after addition of 1% SDS, diluted 10 fold with 450 μL IP buffer (100 mM NaCl, 50 mM Hepes, pH 7.4, 1% Triton X-100) and incubated with 1µg of anti-α-tubulin (Sigma T6199) or anti-β-tubulin (Sigma T7816) antibody and 5 μL of protein G agarose at 4 °C for 2 hours. Beads were washed four times with 400 μL IP buffer and eluted with protein sample buffer for SDS-PAGE gel electrophoresis and autoradiography.

Cryo-EM grid preparation and data collection

Affinity-purified TTC5-RNCs were adjusted to ~ 100 nM (A_{260} of 6) with PSB and vitrified on UltrAuFoil R2/2 300-mesh grids (Quantifoil) coated with graphene oxide (Sigma). Briefly, grids were rinsed in deionized water, air-dried and glow-discharged for 4 min using an Edwards S150B sputter coater at 0.1 torr and 30 mA. 3 μL of 0.2 mg/mL graphene oxide suspension (Sigma Cat #763705-100ML) was overlaid for 1 min, blotted on filter paper and washed three times in deionised water (twice from the sample side, once from the back) and air-dried. 3 µL of sample was pipetted onto graphene oxide-coated grids, incubated for 30 s, blotted using Whatman filter paper grade 597 for 4 s with a blot force of -15 and plunge-frozen in liquid ethane at 92 K using a Vitrobot Mark IV (Thermo Fisher Scientific). Grids were stored in liquid nitrogen until use. The dataset was recorded on a FEI Falcon III camera in integrated mode on a Titan Krios G3 microscope using EPU software. The dataset contained 2805 movies (39 frames; a dose of 1.25 e- frame-1 Å-2; 1s exposure; 59,000X magnification), resulting in a pixel size of 1.339 Å (refer to Table S1 for data statistics).

Cryo-EM data processing

All data processing steps were performed in RELION-3 (*38*). Movies were aligned as 9 x 9 patches using MotionCor2 (*39*) with dose-weighting. Contrast transfer function (CTF) was estimated using CTFFIND-4.1 (*40*) and 2669 micrographs with good CTF (and corresponding to a CTF figure of merit > 0.3 and maximum resolution better than 5 Å) were selected for further processing. 234,788 particles were picked using a 20 Å lowpass-filtered 80S ribosome 3D reference and extracted in a 400-pixel box, which was then downscaled into a 128 pixel box (4.16 Å/pixel). Following visual confirmation of the high quality of data, 2D classification was bypassed and initial three-dimensional refinement was carried out using a 70 Å lowpass-filtered map of a rabbit ribosome as reference to yield a starting ribosome map at Nyquist resolution (8.44 Å) with an estimated angular accuracy of 0.75°. Clear density was visible near the nascent chain tunnel exit for factors later identified as TTC5 and nascent chain-associated complex (NAC).

To enrich for populations containing these factors, focused classification with partial signal subtraction (FCwSS) was performed on the data with soft masks to protect the

factors while subtracting signal corresponding to the rest of the ribosome. 3D-classification without alignment of the subtracted particles into 5 classes yielded a class of active 80S ribosomes with a P-site tRNA and strong density for TTC5 and NAC (23%, 54,865 particles) and this subset was refined to an angular accuracy of 0.67°, re-extracted in a 400-pixel box (1.339 Å/pixel) and re-refined to 0.43° angular accuracy and 3.72 Å resolution. A second class (64%, 149,936 particles) containing NAC density but not TTC5 density was also obtained and presumably represents particles that had lost TTC5 during vitrification. This class was refined to an angular accuracy of 0.7°, re-extracted in a 400-pixel box (1.339 Å/pixel) and re-refined to 0.4° angular accuracy and 3.3 Å resolution. Particles in the TTC5-containing class were next subjected to Bayesian polishing and 3D refinement, which improved the resolution to 3.57 Å.

Because density for the 40S was smeared due to a mixture of subunit rotation states, we subtracted the 40S and focused on the 60S-TTC5 regions of the map. This step resulted in an improved resolution of 3.3 Å. A second round of FCwSS on TTC5 density was performed on the polished, 40S-subtracted particles (which eliminated ~ 3% of particles) and CTF refinement was performed to improve estimations of beamtilt, per-particle defocus and per-particle astigmatism. These steps resulted in an improved angular accuracy of 0.34° and a final, gold-standard resolution of 3.1 Å.

Local resolution and map quality of TTC5 and the bound tubulin nascent chain residues suffered from some degree of flexibility of TTC5 relative to the ribosome. To improve the alignment, we therefore also performed focussed 3D refinement of TTC5 density with signal from the ribosome subtracted. Briefly, TTC5 density was masked, centered and re-extracted in a 200-pixel box (1.339 Å/pix) and signal from the 60S was subtracted. The particles were then refined with a local angular search of 0.9° to minimize overfitting and prevent diverging angular assignments. The resulting map (fig. S5A) was at a modest resolution of 6.8 Å but had clear density in the nascent chain binding pocket.

Model building, refinement and validation

To build a model for the TTC5-bound ribosome, rRNA, P-site tRNA and protein chains from the 60S of PDB 5LZS (*41*) were first docked into the sharpened, modulation transfer function (MTF)-corrected density. Clear, unambiguous density was visible for the β-tubulin nascent chain inside the ribosome exit tunnel (residues 37-64) and this region was modelled *de novo*. The bond between the 3'O of A76 of the P-site tRNA and the carbonyl C of valine 64 was added as a custom bond geometric restraint via an additional parameter input file during refinement in phenix.real_space_refine. Density for the TTC5-bound residues 1-8 of nascent β-tubulin was observed at a lower resolution owing to flexibility of TTC5 relative to the 60S. These residues were therefore modelled conservatively as Cβ stubs and held in place during real-space refinement via an additional reference model input file. A TTC5 homology model based on the crystal structure of mouse TTC5 [PDB 4ABN; (*42*)] was derived using SWISS-MODEL (*43*), and adjusted to fit the density using ProSMART restraints in Coot (*44*, *45*). The NAC model was derived from PDB 3MCB (*46*). A putative N-terminal extension of NACα that is not seen in previous NAC structures was observed to insert between ribosomal proteins eL19 and eL22 and was modeled as poly-Ala. The overall model was adjusted manually in Coot to conform with the density using suitably blurred maps (with B-factors between

0 and 100), saved in mmCIF/PDBx format and real space-refined using phenix.real_space_refine. The 40S was simply modeled in the canonical state via structural superimposition of PDB 5LZS. Model statistics (Table S1) were generated automatically using Molprobity via the Phenix GUI (*47*). All reported resolutions are based on the Fourier shell correlation (FSC) 0.143 criterion (*48*).

Molecular graphics

Structural figures were generated using Pymol (Schrödinger, LLC) and UCSF Chimera (*49*). The FSC curve was generated in Microsoft Excel and annotated in Adobe Illustrator.

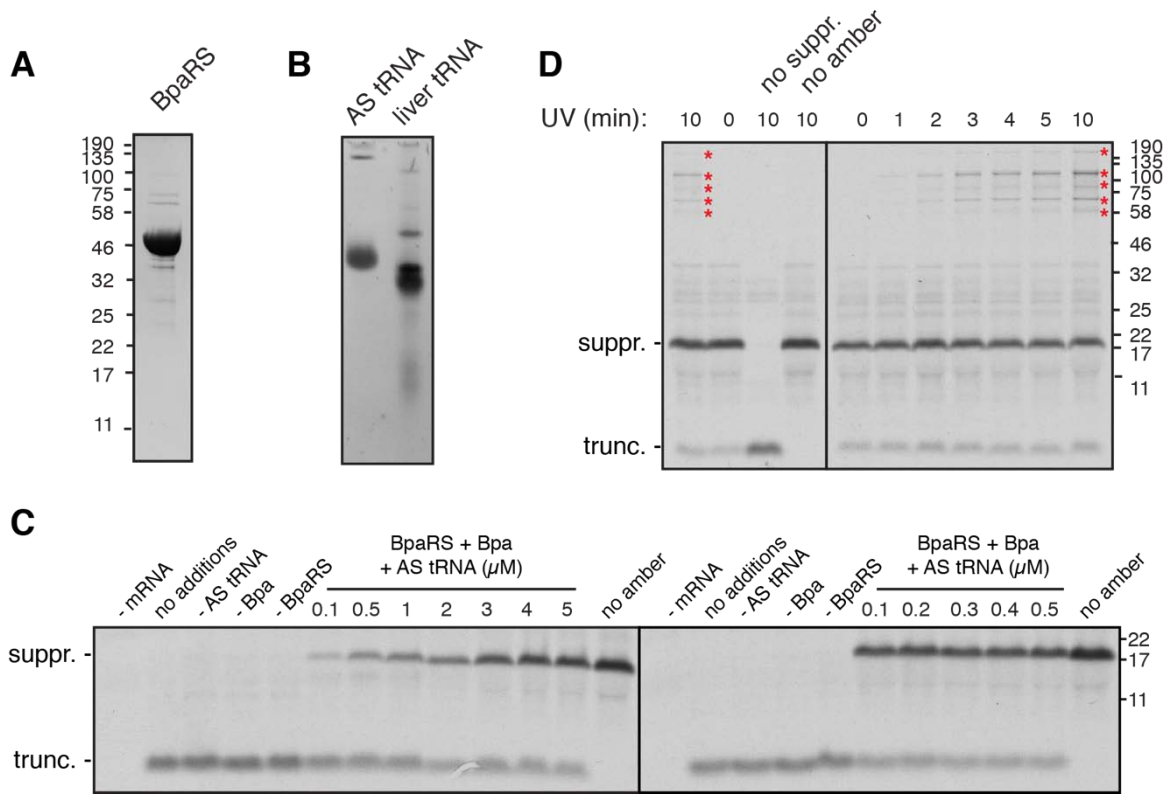

Fig. S1 - Characterization of amber-suppressor mediated photo-crosslinking in vitro
(A) Coomassie stained gel of purified tRNA synthetase (BpaRS) for charging of benzoyl-phenylalanine (Bpa). (B) Stained acrylamide gel of in vitro transcribed and purified amber-suppressor tRNA (AS tRNA) compared to a comparable amount of total porcine liver tRNA. (C) In vitro translation in rabbit reticulocyte of a ^{35}S-labelled 143 amino acid protein (encoding the N-terminal fragment of the β1-adrenergic receptor) containing an amber codon at position 52 (within the first transmembrane domain). The first lane of each panel lacks mRNA, and the last lane of each panel contains a version of the construct lacking the amber codon. Other lanes contained various combinations of Bpa, BpaRS, and AS tRNA as indicated. The positions of the truncated product (i.e., terminated at the amber codon) and the amber-suppressed product are indicated. (D) Translation reactions of the amber containing protein from panel C were performed with Bpa, BpaRS, and AS tRNA under optimized conditions as identified in panel C. Lane 3 lacks the components for amber suppression, and lane 4 contains mRNA for a matched protein lacking an amber codon. After the translation reaction, the samples were irradiated with UV light for the indicated times. The positions of suppression-dependent and UV-dependent crosslinking partners are indicated by red asterisks. These are cytosolic chaperones that interact with the transmembrane domain of the translation product.

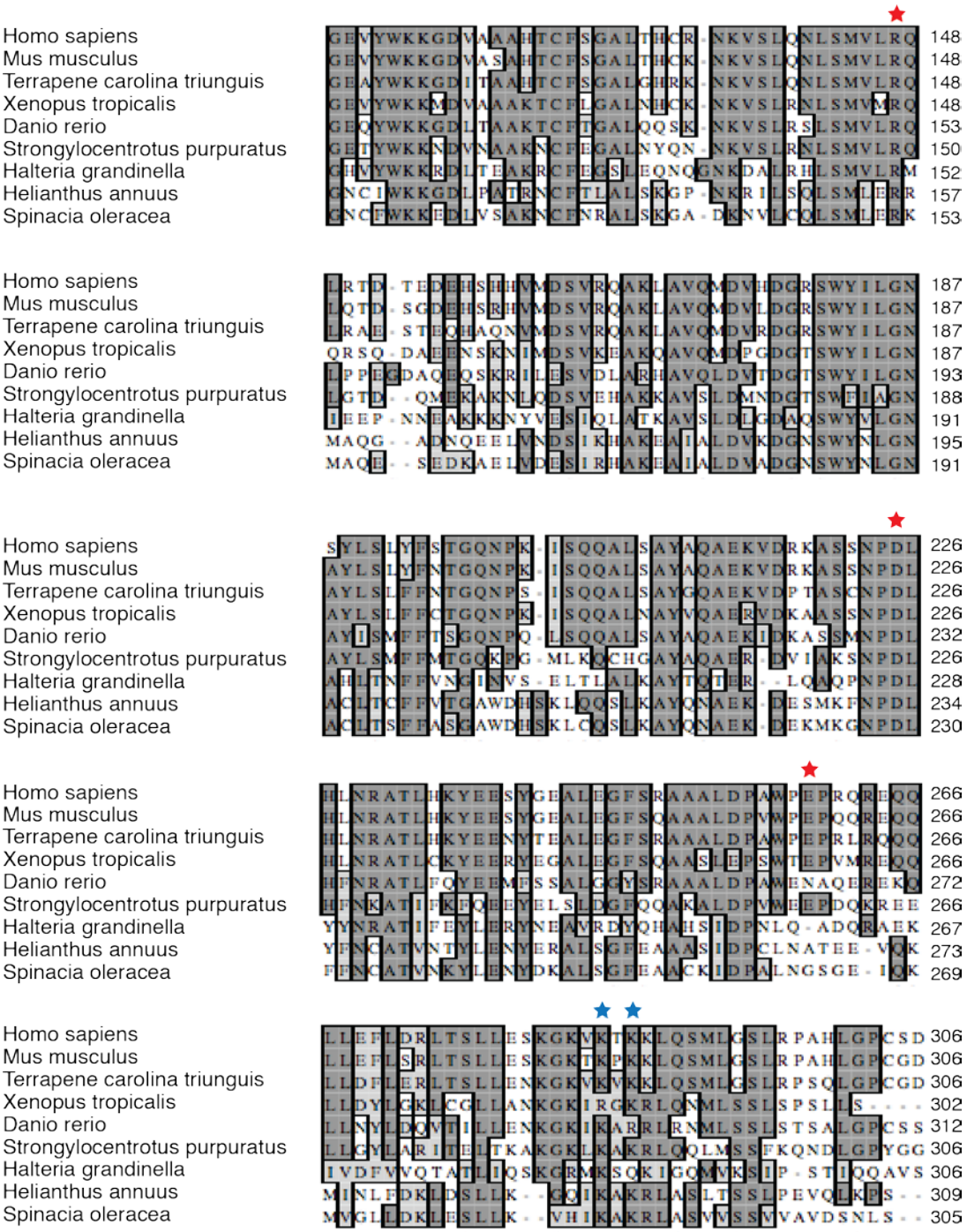

Fig. S2 - Multiple sequence alignment of TTC5 from several species by ClustalW

The residues of human TTC5 that were mutated to disrupt its interaction with tubulin nascent chains or the ribosome are indicated by red and blue asterisks, respectively. The common names of the species that are shown are, in order, human, mouse, turtle, frog, zebrafish, sea urchin, spirotrich ciliate, sunflower, and spinach.

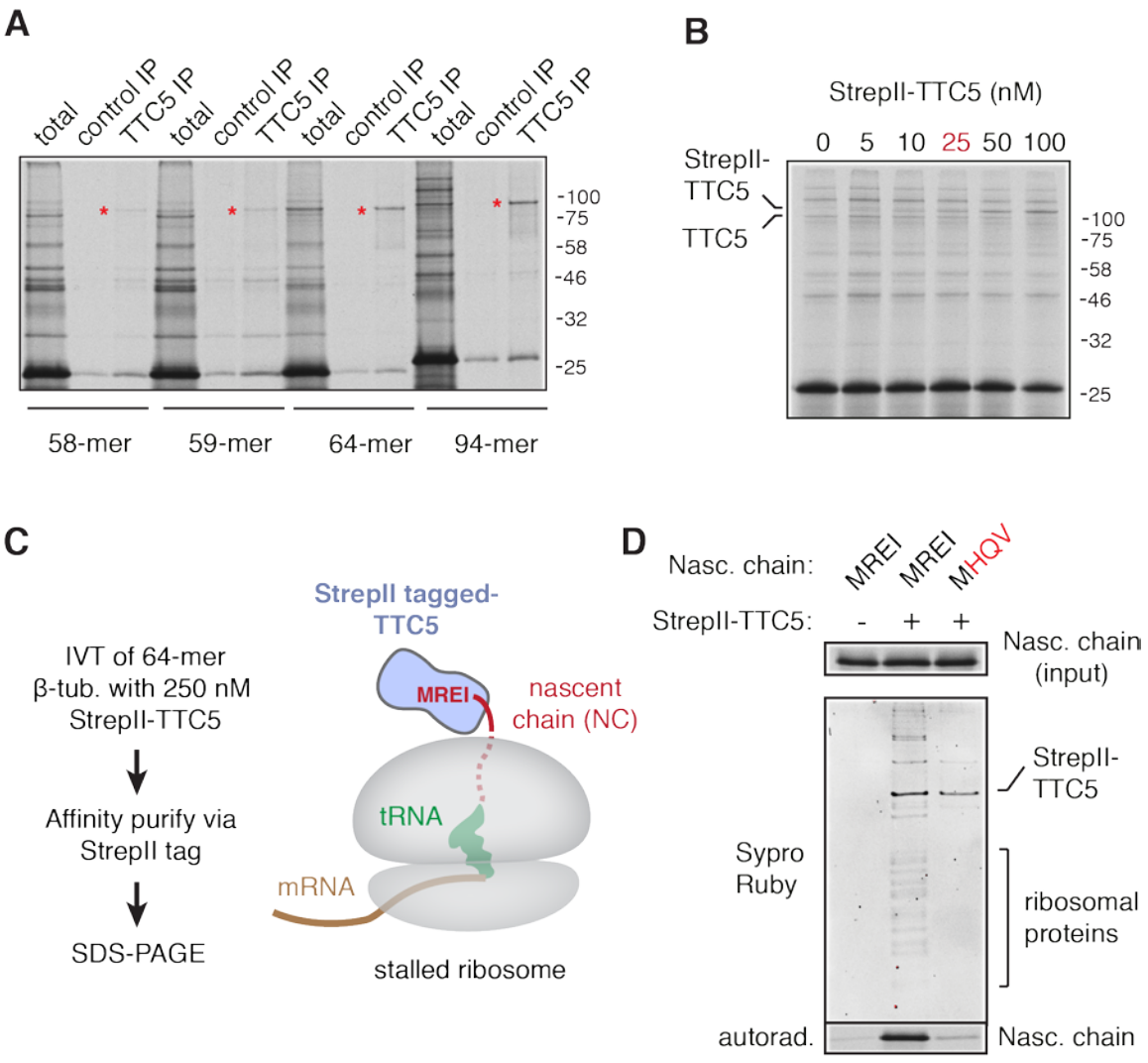

Fig. S3 - Preparation of a ribosome-nascent chain (RNC) complex with TTC5

(A) Analysis of TTC5 crosslinking to different lengths of nascent β-tubulin shows maximal crosslinking at 64 amino acids or longer. Crosslinking analysis was performed as depicted in Fig. 1A. For each length, an aliquot of the total crosslinking reaction is shown together with immunoprecipitation (IP) using control or TTC5 antibodies. Red asterisks indicate the TTC5 crosslink. (B) Titration of recombinant StrepII-tagged TTC5 into the reticulocyte lysate translation reaction and analysis by photo-crosslinking as in Fig. 1B. Endogenous TTC5 is competed by recombinant TTC5, with ~50% competition at 25 nM. (C) Experimental strategy based on the results from panels A and B to assemble and purify the TTC5-RNC complex for cryo-EM analysis. (D) Analysis of TTC5-RNC purifications performed using nascent chains containing wild type or mutant β-tubulin. Ribosomes and the nascent chain are only recovered in the StrepII-based affinity purification when StrepII-TTC5 is included in the reaction. Recovery is lost if the N-terminus of β-tubulin is mutated. Note that crosslinking was not used because the TTC5-RNC complex remained stable during the purification.

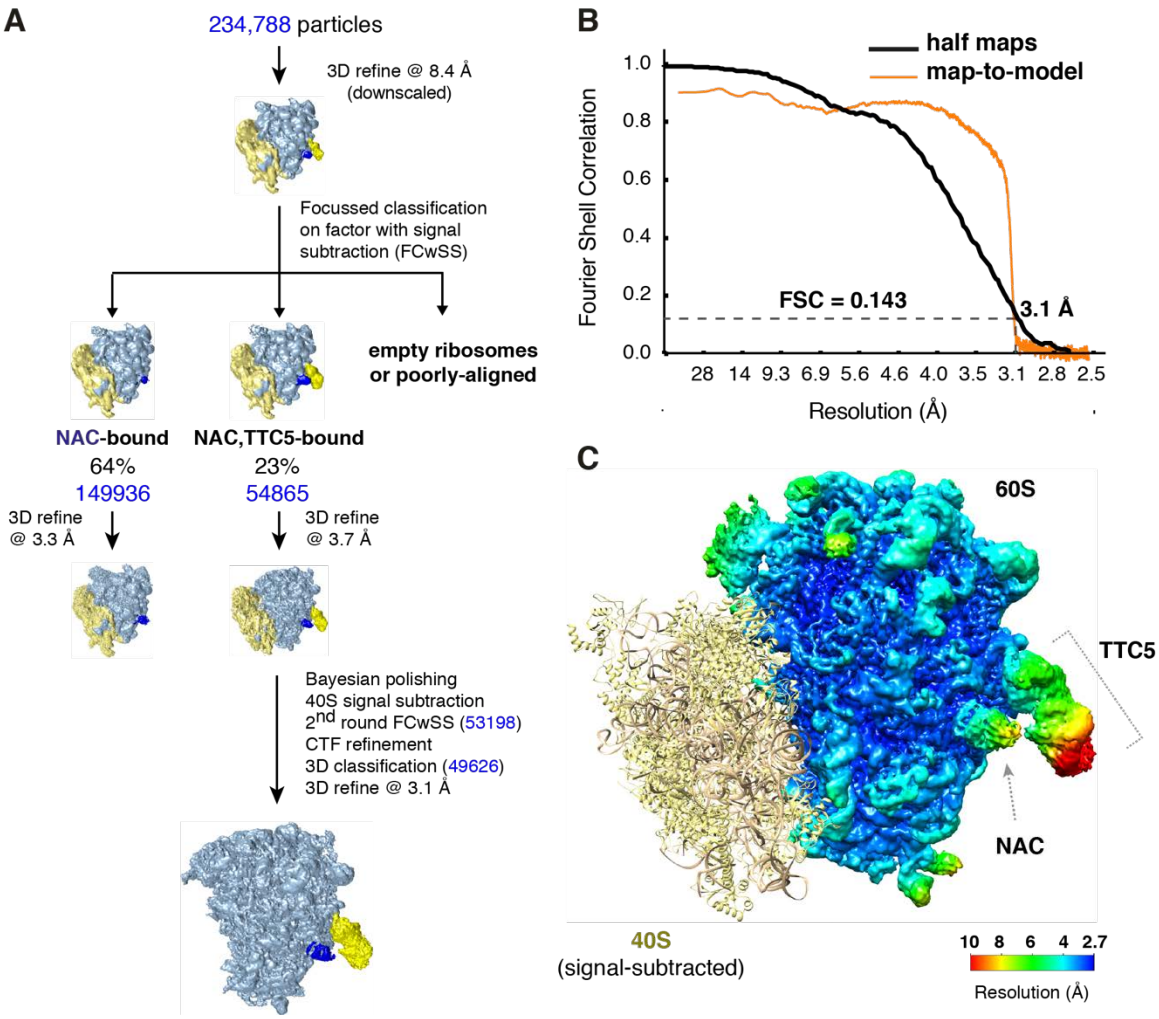

Fig. S4 - Cryo-EM analysis of the TTC5-RNC complex

(A) Classification and reconstruction scheme of ribosomal particles from the EM micrographs. (B). Fourier shell correlation curves for the independent half maps of the 60S-TTC5 reconstruction (black) and between the final map and refined model (orange). (C) Local resolution of the 60S-TTC5 map. The sites of direct interaction between TTC5 and the ribosome were at ~3 to 3.5 Å resolution. The remainder of TTC5 varied in resolution, but was sufficient to dock a previous crystal structure of mouse TTC5 and make minor adjustments as necessary (see Fig. S5). The ubiquitous ribosome binding protein NAC was observed in our reconstructions but was not investigated or analyzed further in this study.

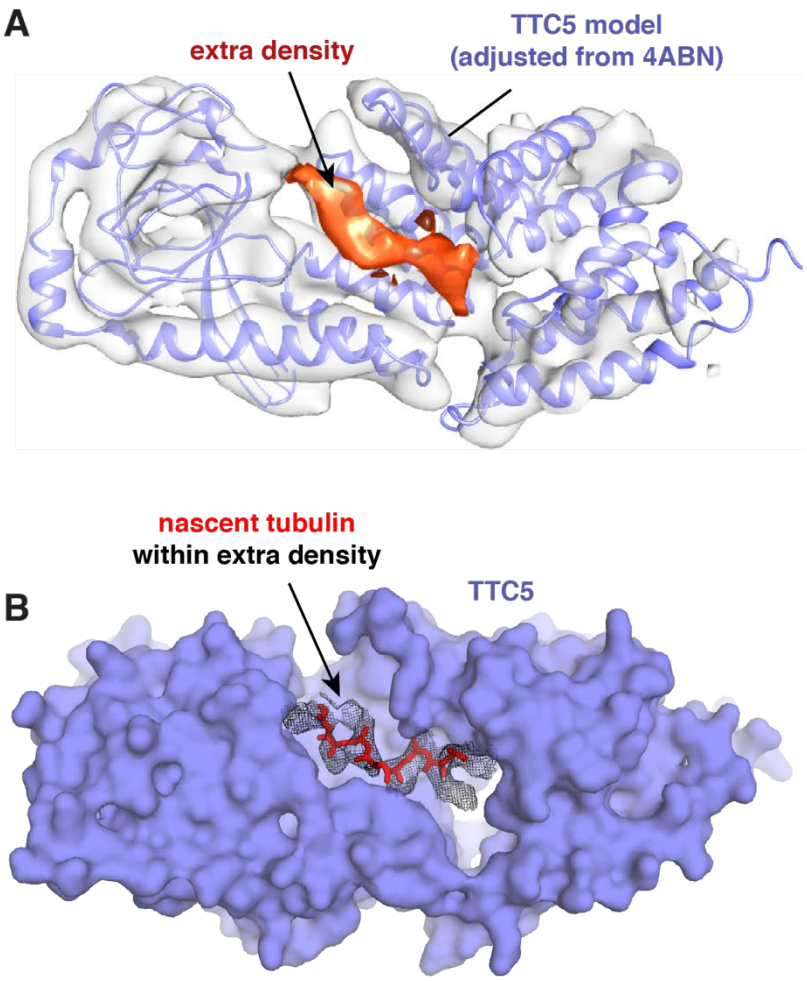

Fig. S5 - Experimental density for nascent tubulin within TTC5

(A) Shown is the unsharpened density map for TTC5 fitted with the human TTC5 homology model adjusted from the crystal structure of mouse TTC5 (4ABN). Additional density (orange) that is not accounted by TTC5 is shown inside the putative binding groove. (B) Space-filling model of TTC5 with the sharpened density within the groove shown in wire mesh. The model for the backbone of β-tubulin with C-β atoms for side chains is shown in red.

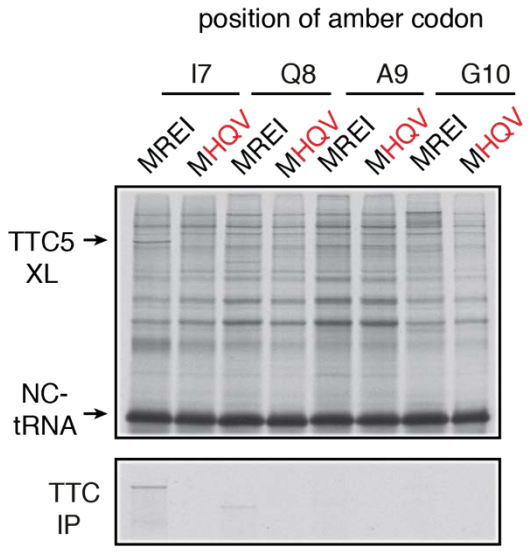

Fig. S6 – Position-dependent crosslinking of TTC5 to nascent β-tubulin

Codon 7, 8, 9 or 10 of β-tubulin was replaced with an amber codon in order to incorporate the UV crosslinking unnatural amino acid Bpa at that position. The crosslinking products were immunoprecipitated by TTC5 antibody. Very poor crosslinking from position 8 and no crosslinking from positions 9 and 10 are seen. This result is consistent with the assignment of β-tubulin within the TTC5 binding groove. Note that crosslinked products often migrate anomolously on SDS-PAGE, as seen for the crosslink to TTC5 from position 7 versus position 8.

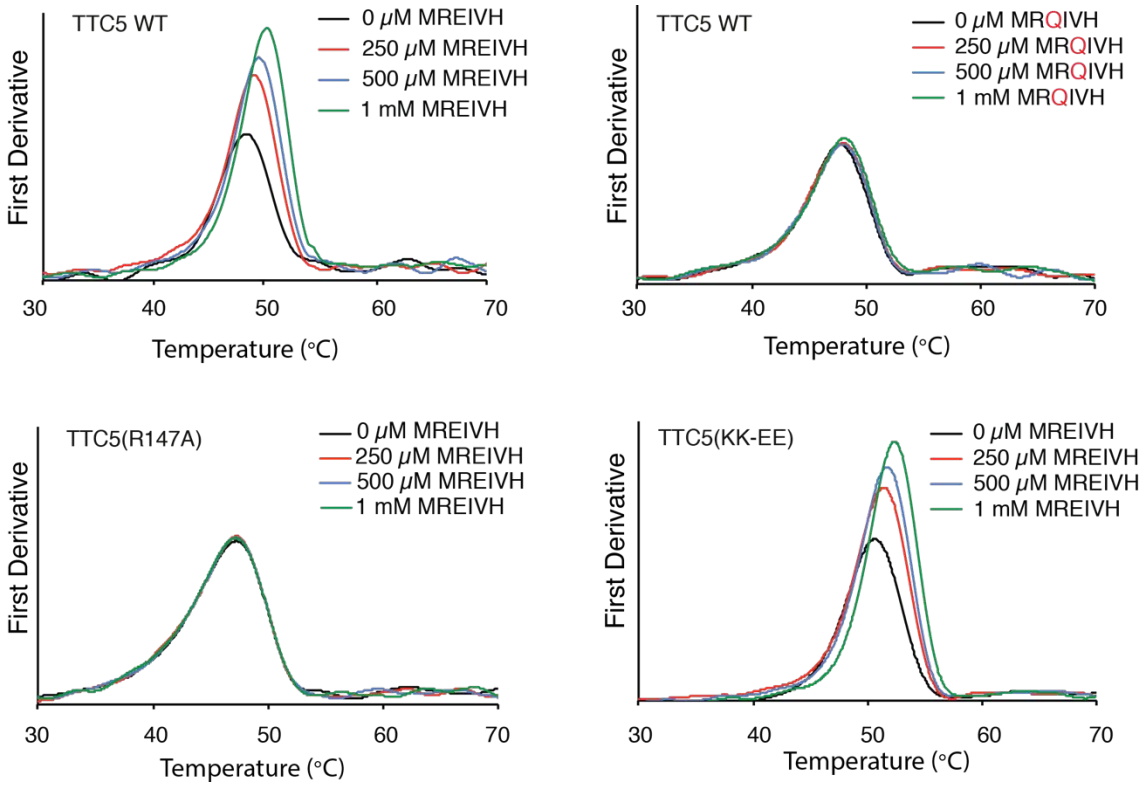

Fig. S7 - Recombinant TTC5 binding to β-tubulin peptides

The binding interaction between recombinant TTC5 and a synthetic peptide of the first six amino acids of β-tubulin was analysed by a thermal shift assay in which denaturation of TTC5 is monitored by intrinsic tryptophan fluorescence. Each plot shows the first derivative of the denaturation curve. The peak represents the inflection point of the sigmoidal denaturation curve. The indicated combinations of recombinant TTC5 and peptide were mixed and subjected to progressive temperature shifts. The denaturation temperature of recombinant wild type TTC5 is shifted by wild type β-tubulin peptide (upper left panel). Exactly the same result was seen for the ribosome binding deficient mutant TTC5 (KK-EE). Mutating either the peptide (upper right) or the binding pocket of TTC5 (i.e., R147A; lower left) completely abolished the interaction. The interactions tabulated in Fig. 3C were determined in exactly the same manner and showed either wild type level of binding or no detectable binding as indicated in the table.

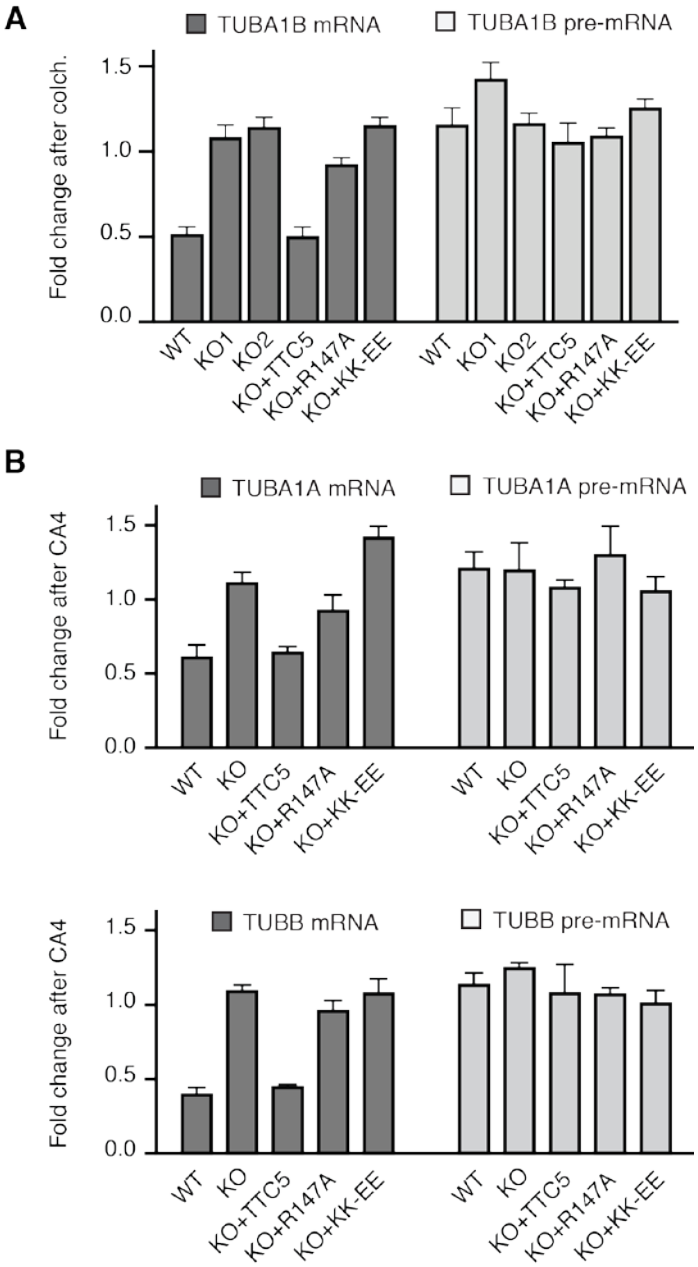

Fig. S8 - Tubulin mRNA degradation requires TTC5 at the ribosome

(A) The indicated HEK293 cell lines were either left untreated or treated for 3 h with colchicine. The relative amounts of the indicated mRNAs or pre-mRNAs were quantified by RT-qPCR and normalized to a control ribosomal RNA. The fold-change after colchicine treatment relative to the untreated sample for each cell line is plotted (mean ± SEM from three replicates). (B) The indicated HeLa cell lines were either left untreated or treated for 4 h with combretastatin A4 (CA4). The relative amounts of the indicated mRNAs or pre-mRNAs were quantified by RT-qPCR and normalized to a reference gene (GAPDH). The fold-change after CA4 treatment relative to the untreated sample for each cell line is plotted (mean ± SEM from three replicates).

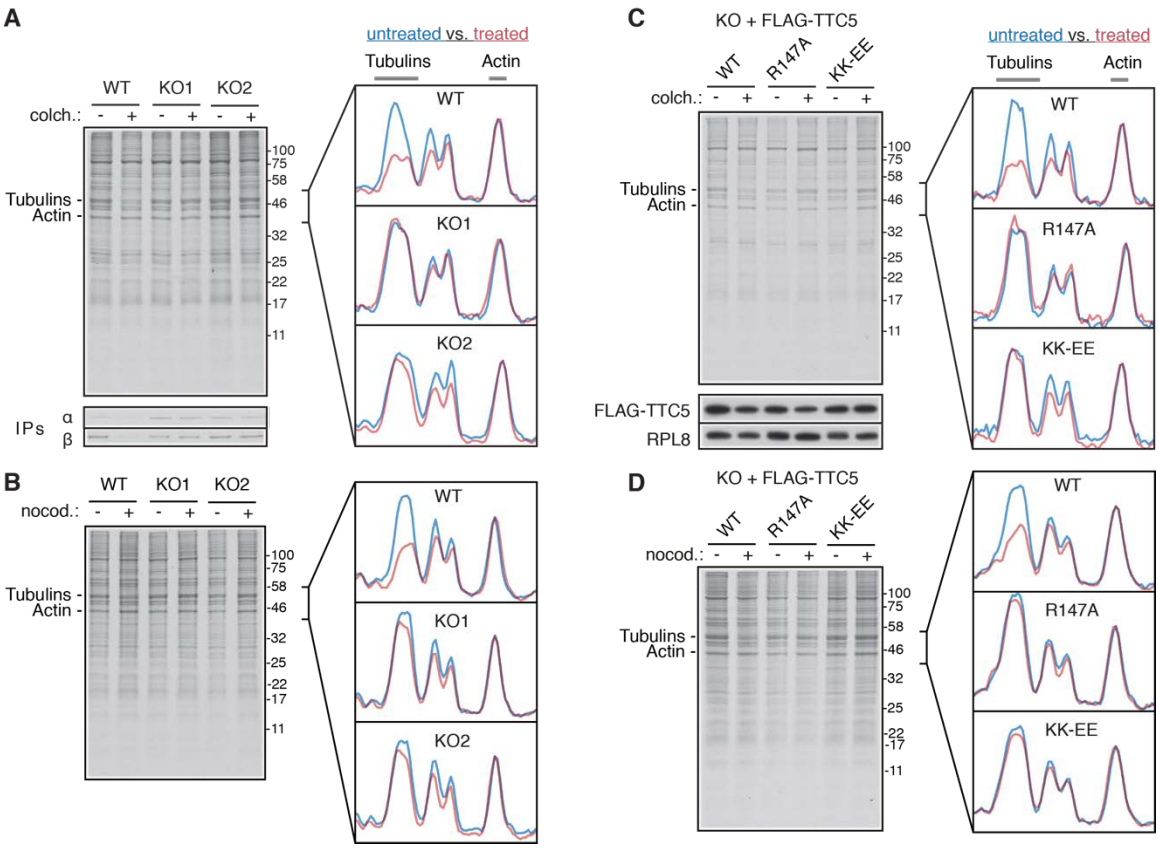

Fig. S9 - TTC5 is required for tubulin autoregulation

(A-D)The indicated HEK293 cell lines were either left untreated or treated for 3 h with colchicine (colch.) or nocodazole (nocod.) before pulse-labelling for 30 min with ^{35}S-methionine. The total products were visualized by autoradiography. The indicated region of the autoradiograph containing tubulins and actin was analyzed by scanning densitometry. The traces, normalized to the actin band, are shown from untreated (blue) and nocodazole-treated (red) samples for each cell line. Autoregulation is only seen in cells containing wild type TTC5.

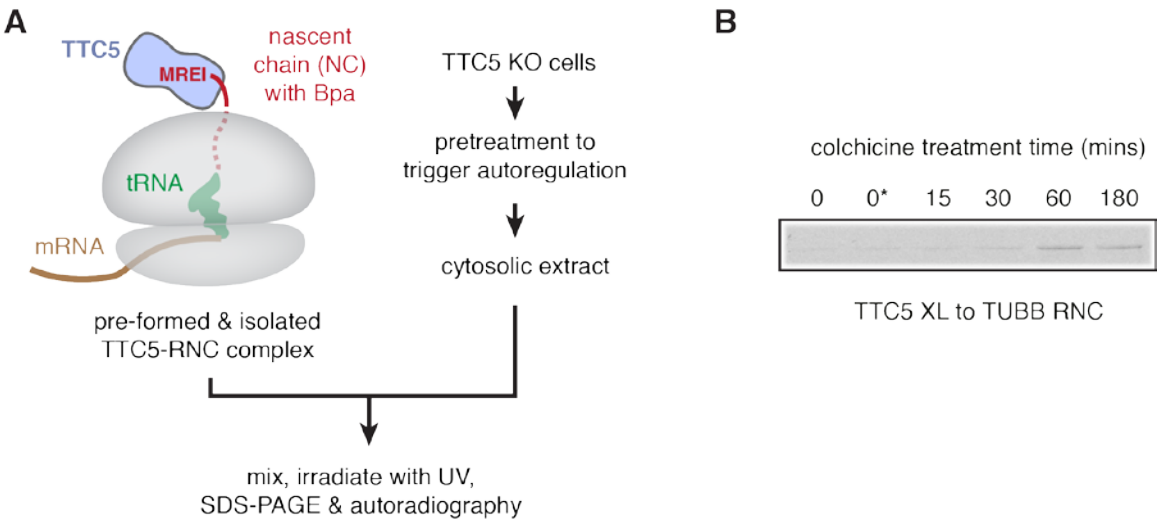

Fig. S10 - Detection of a TTC5 inhibitor that is lost in colchicine-treated cells

(A) Diagram depicting the protocol for the experiments shown in Fig. 4B and fig. S10B. ^{35}S-labelled 94-mer β-tubulin nascent chain containing Bpa at position 7 is prepared in reticulocyte lysate (as in Fig. 1A) and the RNC-TTC5 complex is isolated by centrifugation. This pre-formed RNC-TTC5 complex is then mixed with cytosolic lysate from TTC5 knockout cells that had been pre-treated (+col) or not (-col) with colchicine for up to 3 hours to initiate autoregulation. TTC5 knockout cells were used to ensure that the only TTC5 in the reaction was from the pre-formed TTC5-RNC complex. While autoregulation cannot be executed in these cells due to the absence of TTC5, we reasoned that cells would still trigger the process. The samples are then subjected to UV crosslinking to monitor the nascent chain interactions. (B) An experiment similar to Fig. 4B (and diagrammed in fig. S10A) was performed and the TTC5 crosslinked product was recovered by immunoprecipitation via TTC5. Shown is the autoradiograph visualizing the TTC5-nascent chain crosslinked product. Lysate from untreated cells completely disrupts the TTC5-RNC interaction, so no crosslinked product is seen. When cells are pre-treated with colchicine, the inhibitory activity that disrupts the TTC5-RNC interaction is progressively lost, and the crosslink is observed. This suggests that untreated lysate contains an inhibitor of the TTC5-RNC interaction that is not active or not present in the colchicine-treated lysate. One of the control samples included colchicine added after cell lysis (indicated as 0*). This post-lysis treatment did not inactivate the inhibitor, which is only inactivated over time when the autoregulation signal is initiated in live cells.

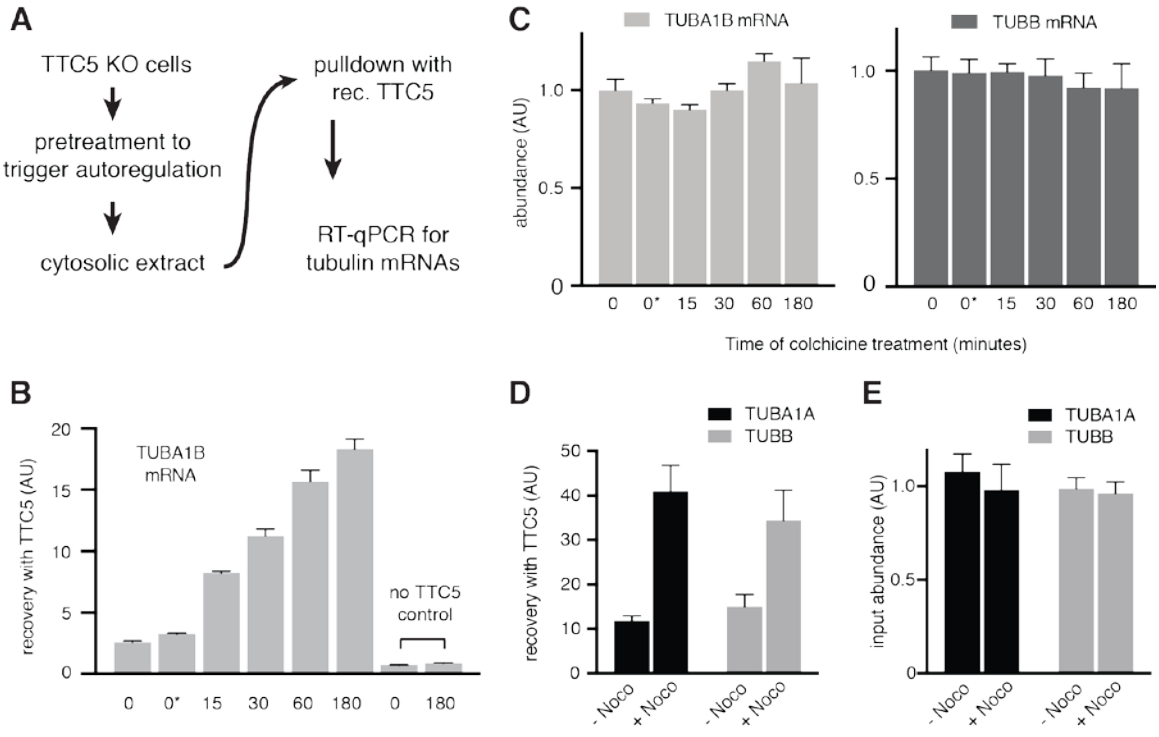

Fig. S11 - TTC5 engages tubulin mRNAs preferentially during autoregulation

(A) Experimental strategy for Fig. 4C and fig. S10B. TTC5 knockout cells were used to ensure that tubulin mRNA content does not change during the experiment (verified in fig. S11C). While autoregulation cannot be executed in these cells due to the absence of TTC5, we reasoned that cells would still trigger the process. (B) TTC5-knockout HEK293 cells were pre-treated for the indicated times with colchicine and used to prepare lysates (as in Fig.4C). One of the control samples included colchicine added after cell lysis (indicated as 0*). Each lysate was incubated with immobilized recombinant TTC5 and the recovered products were analyzed for the indicated α- and β-tubulin mRNAs by quantitative RT-PCR. The relative recoveries of tubulin mRNAs to a ribosomal protein mRNA are plotted (mean ± SD from three biological replicates). Control pulldowns using resin lacking TTC5 were analyzed in parallel. (C) Aliquots of the same lysates prepared for panel A and Fig. 4C were analyzed for total α- and β-tubulin mRNAs by quantitative RT-PCR. The abundances of tubulin mRNAs relative to a ribosomal protein mRNA are plotted (mean ± SD from three replicates). As expected for TTC5 knockout cells, neither alpha nor beta tubulin mRNAs change their abundance during this time of colchicine treatment. (D) TTC5-knockout HEK293 cells were left untreated or pre-treated with nocodazole for 15 minutes and used to prepare lysates. Each lysate was incubated with immobilized recombinant TTC5 and the recovered products were analyzed for the indicated α- and β-tubulin mRNAs by quantitative RT-PCR. The relative recoveries of tubulin mRNAs to a ribosomal protein mRNA are plotted (mean ± SD from three biological replicates). (E) Aliquots of the input lysates prepared in panel D were analyzed for total α- and β-tubulin mRNAs by quantitative RT-PCR. The abundances of tubulin mRNAs relative to a ribosomal protein mRNA are plotted (mean ± SD from three biological replicates).

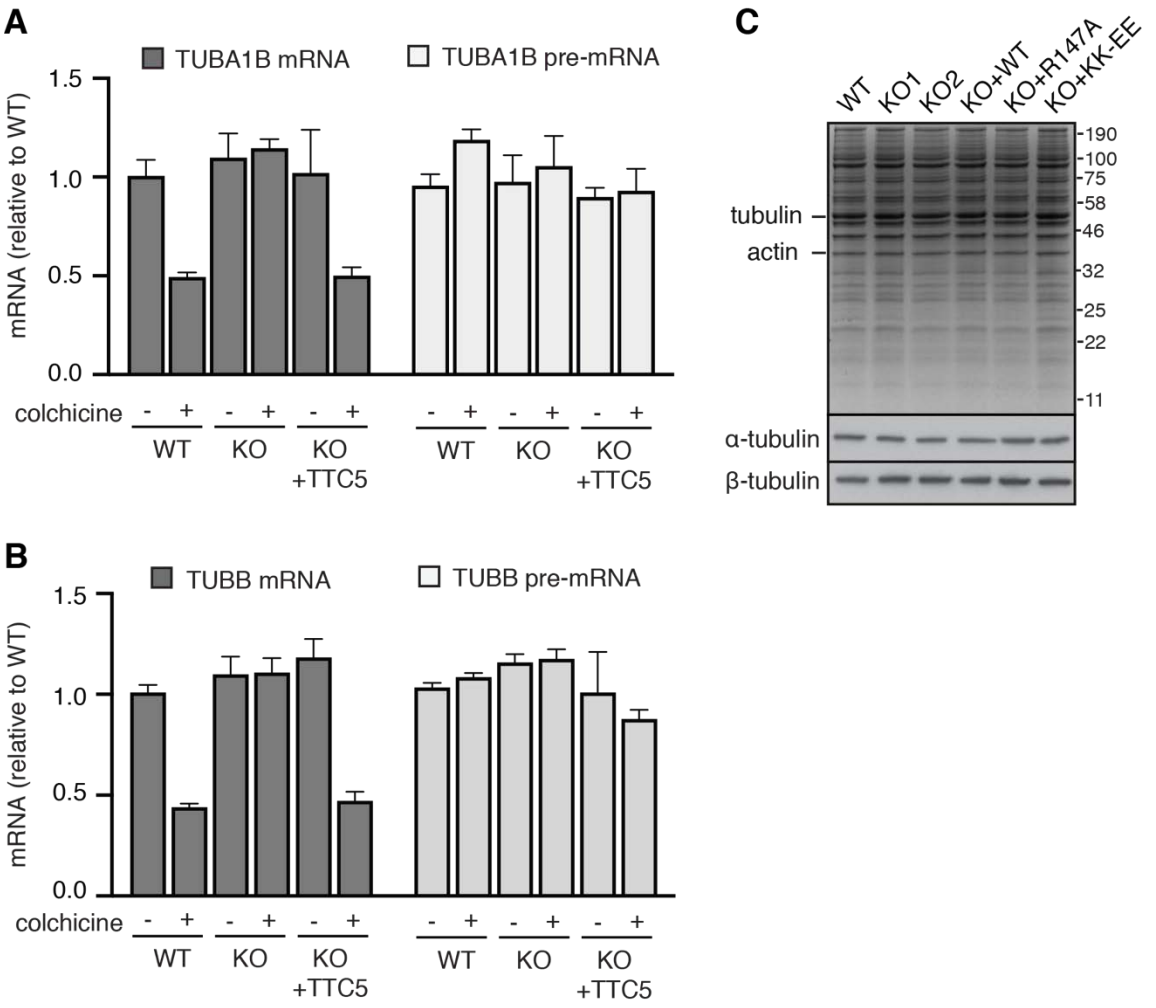

Fig. S12. TTC5 knockout cells have normal tubulin mRNA and protein levels

(A, B) The indicated HEK293 cell lines were either left untreated or treated for 3 h with colchicine. The relative amounts of α-tubulin (panel A) and β-tubulin (panel B) mRNAs or pre-mRNAs were quantified by RT-qPCR and normalized to a control ribosomal RNA. Plotted is the mean ± SD from three biological replicates. Note that relative to wild type cells (arbitrarily set at 1), the tubulin mRNA levels are not appreciably changed in TTC5 knockout (KO) cells or in KO cells rescued by TTC5 re-expression. As expected, colchicine treatment of WT and KO+TTC5 results in ~2-fold reduction in mRNA (but not pre-mRNA). (C) The upper panel shows Coomassie staining of total proteins in lysates from the indicated HEK293 cell lines. An aliquot of the lysates was blotted with the indicated tubulin antibodies (bottom panels). No obvious difference in steady state tubulin levels was observed across the different cell lines. Because these measurements of total tubulin mRNA and protein were on unsynchronized bulk cultures (where the vast majority of cells are not undergoing mitosis at any given moment), subtle differences selectively during mitosis would not be apparent. Future work will be needed to directly measure various aspects of tubulin dynamics either in synchronized cultures or in single cells to determine how the absence of autoregulation perturbs tubulin to impact mitosis.

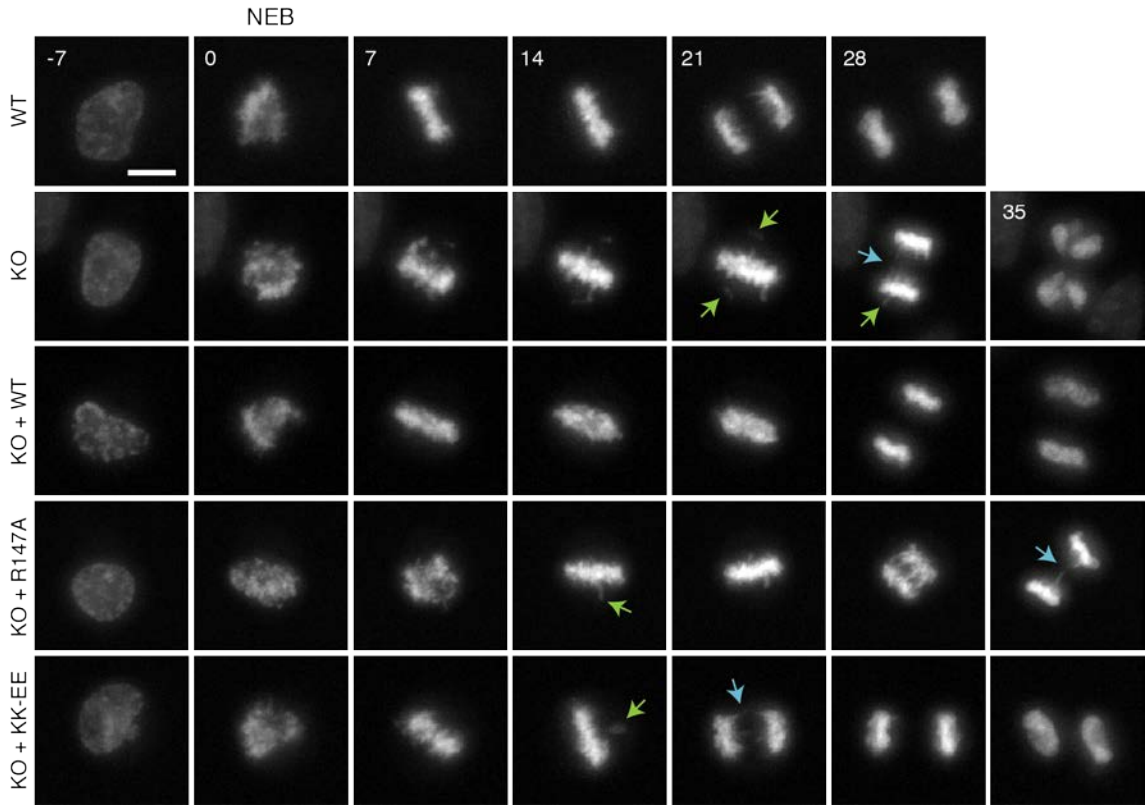

Fig. S13 - Loss of TTC5 compromises mitotic fidelity

Examples of time-lapse images of the indicated HeLa cell lines stained with sirDNA dye. Time (in minutes) relative to nuclear envelope breakdown (NEB) is shown in the upper left of images. Green arrows indicate examples of errors in chromosome alignment onto the metaphase plate. Blue arrows indicate errors in chromosome segregation in anaphase. Scale bar = 5 μm.

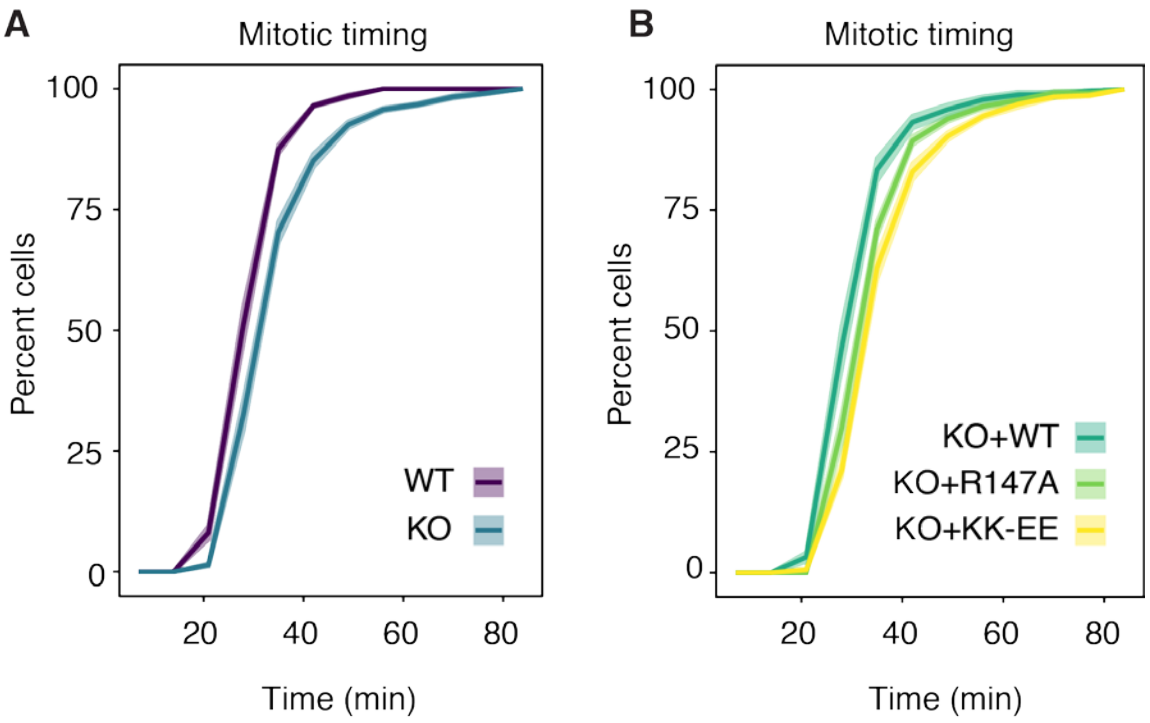

Fig. S14 - Loss of TTC5 delays mitotis

Cumulative frequency of mitotic duration time (from nuclear envelope breakdown to telophase) for the indicated HeLa cell lines. Plotted is the percent of cells that have completed mitosis at each time point. Full lines represent average cumulative frequency, and shaded areas are SEM from 4-6 independent biological replicates and 200-400 analyzed cells.

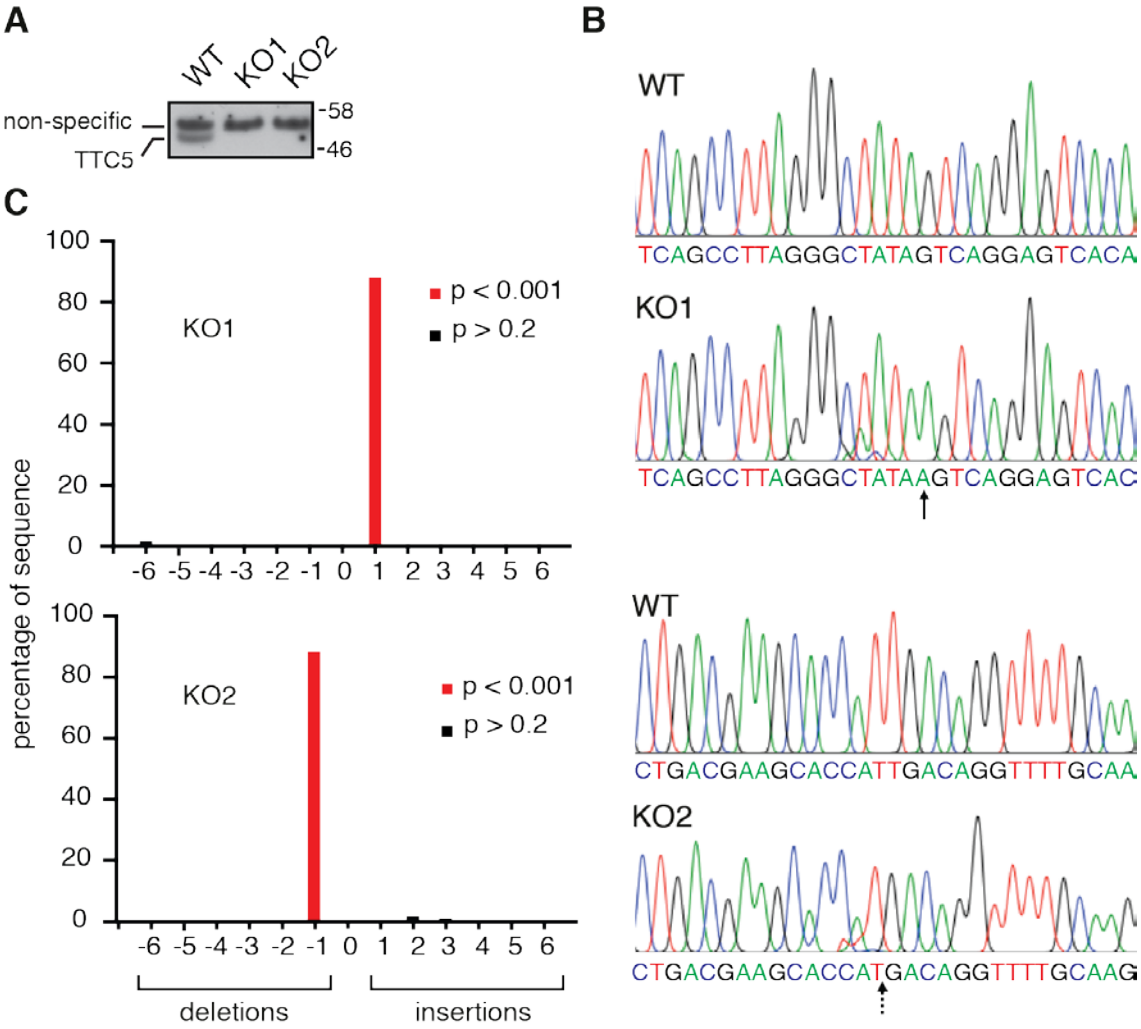

Fig. S15 - Validation of TTC5 knockout cells

(A) Anti-TTC5 western blot analysis of total lysate obtained from WT HEK293 cells or each of two independently derived TTC5-knockout cells generated with different guide RNAs. (B) Genotyping of TTC5-knockout cells. The modified genomic region was amplified via PCR and sequenced. The chromatograms of the amplicons from wild type and TTC5-knockout cells are shown, with arrow indicating the site of a single base insertion (KO1) and single base deletion (KO2). (C) The chromatograms for the knockout cells in panel B were compared to that from WT cells using Tracking of Indels by DEcomposition (TIDE) analysis. The knockout alleles in KO1 are +1 frameshifted and the alleles in KO2 are -1 frameshifted. HeLa cell knockouts were similarly verified.

Table S1.

Data collection, processing, refinement and model statistics.

Data Collection	
Microscope	Titan Krios
Voltage (kV)	300
Magnification (corrected)	104,555
Pixel size (Å)	1.339
Detector	Falcon III
Defocus range (μm)	-0.9 to -2.7
Defocus mean (μm)	-1.8
Total electron exposure (e-Å-2)	48.36
Exposure rate (e-Å-2frame-1)	1.24
Data collection software	EPU
Data Processing	
Independent data collections	1
Useable micrographs	2669
Particles picked	234788
Final particles	49626
Map sharpening B-factor (Å2)	-10
Accuracy translations (pix) / rotations (°)	0.26 / 0.34°
Resolution (Å) Unmasked (0.5 / 0.143 FSC) Masked (0.5/0.143 FSC)	 3.89 / 3.14 3.33 / 2.98
Local resolution range (Å)	13.5-2.7
EMDB accession code	EMD-10380
PDB accession code	6T59
Model Composition	
Chains	53
Non-hydrogen atoms	143,048
Protein residues	7383
RNA bases	3890
Metals (Mg2+/Zn2+)	220/5
Refinement	
Software	phenix.real_space_refine
Resolution (Å)	3.11
CC (mask)	0.87
CC (main chain)	0.86
CC (side chain)	0.86
Average B factors (Å2) Protein Nucleotide	 60.6 94.1
R.M.S deviations	
Bond lengths (Å)	0.011
Bond angles (°)	0.824
Validation	
Molprobity score	2.07
Clashscore, all atoms	10.66
Rotamers outliers (%)	0.68
Cβ outliers (%)	0.00
EMRinger score	3.08
CaBLAM outliers (%)	3.24
Ramachandran plot	
Favored (%)	90.92
Allowed (%)	8.98
Outliers (%)	0.10

References

1. G. Borisy, R. Heald, J. Howard, C. Janke, A. Musacchio, E. Nogales, Microtubules: 50 years on from the discovery of tubulin. *Nat. Rev. Mol. Cell Biol.* **17**, 322–328 (2016). doi:10.1038/nrm.2016.45 Medline

2. A. Desai, T. J. Mitchison, Microtubule polymerization dynamics. *Annu. Rev. Cell Dev. Biol.* **13**, 83–117 (1997). doi:10.1146/annurev.cellbio.13.1.83 Medline

3. G. J. Brouhard, L. M. Rice, Microtubule dynamics: An interplay of biochemistry and mechanics. *Nat. Rev. Mol. Cell Biol.* **19**, 451–463 (2018). doi:10.1038/s41580-018-0009-y Medline

4. R. A. Walker, E. T. O'Brien, N. K. Pryer, M. F. Soboeiro, W. A. Voter, H. P. Erickson, E. D. Salmon, Dynamic instability of individual microtubules analyzed by video light microscopy: Rate constants and transition frequencies. *J. Cell Biol.* **107**, 1437–1448 (1988). doi:10.1083/jcb.107.4.1437 Medline

5. I. Gasic, S. A. Boswell, T. J. Mitchison, Tubulin mRNA stability is sensitive to change in microtubule dynamics caused by multiple physiological and toxic cues. *PLOS Biol.* **17**, e3000225 (2019). doi:10.1371/journal.pbio.3000225 Medline

6. D. W. Cleveland, M. A. Lopata, P. Sherline, M. W. Kirschner, Unpolymerized tubulin modulates the level of tubulin mRNAs. *Cell* **25**, 537–546 (1981). doi:10.1016/0092-8674(81)90072-6 Medline

7. D. W. Cleveland, Autoregulated instability of tubulin mRNAs: A novel eukaryotic regulatory mechanism. *Trends Biochem. Sci.* **13**, 339–343 (1988). doi:10.1016/0968-0004(88)90103-X Medline

8. D. A. Gay, S. S. Sisodia, D. W. Cleveland, Autoregulatory control of β-tubulin mRNA stability is linked to translation elongation. *Proc. Natl. Acad. Sci. U.S.A.* **86**, 5763–5767 (1989). doi:10.1073/pnas.86.15.5763 Medline

9. J. S. Pachter, T. J. Yen, D. W. Cleveland, Autoregulation of tubulin expression is achieved through specific degradation of polysomal tubulin mRNAs. *Cell* **51**, 283–292 (1987). doi:10.1016/0092-8674(87)90155-3 Medline

10. T. J. Yen, P. S. Machlin, D. W. Cleveland, Autoregulated instability of β-tubulin mRNAs by recognition of the nascent amino terminus of β-tubulin. *Nature* **334**, 580–585 (1988). doi:10.1038/334580a0 Medline

11. C. J. Bachurski, N. G. Theodorakis, R. M. Coulson, D. W. Cleveland, An amino-terminal tetrapeptide specifies cotranslational degradation of β-tubulin but not α-tubulin mRNAs. *Mol. Cell. Biol.* **14**, 4076–4086 (1994). doi:10.1128/MCB.14.6.4076 Medline

12. N. G. Theodorakis, D. W. Cleveland, Physical evidence for cotranslational regulation of β-tubulin mRNA degradation. *Mol. Cell. Biol.* **12**, 791–799 (1992). doi:10.1128/MCB.12.2.791 Medline

13. M. Gamerdinger, K. Kobayashi, A. Wallisch, S. G. Kreft, C. Sailer, R. Schlömer, N. Sachs, A. Jomaa, F. Stengel, N. Ban, E. Deuerling, Early Scanning of Nascent Polypeptides inside the Ribosomal Tunnel by NAC. *Mol. Cell* **75**, 996–1006.e8 (2019). doi:10.1016/j.molcel.2019.06.030 Medline

14. R. D. Wegrzyn, D. Hofmann, F. Merz, R. Nikolay, T. Rauch, C. Graf, E. Deuerling, A conserved motif is prerequisite for the interaction of NAC with ribosomal protein L23 and nascent chains. *J. Biol. Chem.* **281**, 2847–2857 (2006). doi:10.1074/jbc.M511420200 Medline

15. B. Wiedmann, H. Sakai, T. A. Davis, M. Wiedmann, A protein complex required for signal-sequence-specific sorting and translocation. *Nature* **370**, 434–440 (1994). doi:10.1038/370434a0 Medline

16. M. Gamerdinger, M. A. Hanebuth, T. Frickey, E. Deuerling, The principle of antagonism ensures protein targeting specificity at the endoplasmic reticulum. *Science* **348**, 201–207 (2015). doi:10.1126/science.aaa5335 Medline

17. UniProt Consortium, UniProt: The universal protein knowledgebase. *Nucleic Acids Res.* **46**, 2699 (2018). doi:10.1093/nar/gky092 Medline

18. J. J. Vicente, L. Wordeman, The quantification and regulation of microtubule dynamics in the mitotic spindle. *Curr. Opin. Cell Biol.* **60**, 36–43 (2019). doi:10.1016/j.ceb.2019.03.017 Medline

19. S. Petry, Mechanisms of Mitotic Spindle Assembly. *Annu. Rev. Biochem.* **85**, 659–683 (2016). doi:10.1146/annurev-biochem-060815-014528 Medline

20. S. L. Prosser, L. Pelletier, Mitotic spindle assembly in animal cells: A fine balancing act. *Nat. Rev. Mol. Cell Biol.* **18**, 187–201 (2017). doi:10.1038/nrm.2016.162 Medline

21. S. L. Kline-Smith, C. E. Walczak, Mitotic spindle assembly and chromosome segregation: Refocusing on microtubule dynamics. *Mol. Cell* **15**, 317–327 (2004). doi:10.1016/j.molcel.2004.07.012 Medline

22. J. T. Lynch, T. D. D. Somerville, G. J. Spencer, X. Huang, T. C. P. Somervaille, TTC5 is required to prevent apoptosis of acute myeloid leukemia stem cells. *Cell Death Dis.* **4**, e573 (2013). doi:10.1038/cddis.2013.107 Medline

23. C. Demonacos, M. Krstic-Demonacos, N. B. La Thangue, A TPR motif cofactor contributes to p300 activity in the p53 response. *Mol. Cell* **8**, 71–84 (2001). doi:10.1016/S1097-2765(01)00277-5 Medline

24. X. Hu, R. D. Mullins, LC3 and STRAP regulate actin filament assembly by JMY during autophagosome formation. *J. Cell Biol.* **218**, 251–266 (2019). doi:10.1083/jcb.201802157 Medline

25. N. Sonenberg, A. G. Hinnebusch, Regulation of translation initiation in eukaryotes: Mechanisms and biological targets. *Cell* **136**, 731–745 (2009). doi:10.1016/j.cell.2009.01.042 Medline

26. J. C. Darnell, E. Klann, The translation of translational control by FMRP: Therapeutic targets for FXS. *Nat. Neurosci.* **16**, 1530–1536 (2013). doi:10.1038/nn.3379 Medline

27. O. Brandman, R. S. Hegde, Ribosome-associated protein quality control. *Nat. Struct. Mol. Biol.* **23**, 7–15 (2016). doi:10.1038/nsmb.3147 Medline

28. C. J. Shoemaker, R. Green, Translation drives mRNA quality control. *Nat. Struct. Mol. Biol.* **19**, 594–601 (2012). doi:10.1038/nsmb.2301 Medline

29. W. F. Marzluff, K. P. Koreski, Birth and Death of Histone mRNAs. *Trends Genet.* **33**, 745–759 (2017). doi:10.1016/j.tig.2017.07.014 Medline

30. B. J. DiDomenico, G. E. Bugaisky, S. Lindquist, The heat shock response is self-regulated at both the transcriptional and posttranscriptional levels. *Cell* **31**, 593–603 (1982). doi:10.1016/0092-8674(82)90315-4 Medline

31. J. W. Chin, T. A. Cropp, J. C. Anderson, M. Mukherji, Z. Zhang, P. G. Schultz, An expanded eukaryotic genetic code. *Science* **301**, 964–967 (2003). doi:10.1126/science.1084772 Medline

32. K. Sakamoto, A. Hayashi, A. Sakamoto, D. Kiga, H. Nakayama, A. Soma, T. Kobayashi, M. Kitabatake, K. Takio, K. Saito, M. Shirouzu, I. Hirao, S. Yokoyama, Site-specific incorporation of an unnatural amino acid into proteins in mammalian cells. *Nucleic Acids Res.* **30**, 4692–4699 (2002). doi:10.1093/nar/gkf589 Medline

33. F. A. Ran, P. D. Hsu, J. Wright, V. Agarwala, D. A. Scott, F. Zhang, Genome engineering using the CRISPR-Cas9 system. *Nat. Protoc.* **8**, 2281–2308 (2013). doi:10.1038/nprot.2013.143 Medline

34. J. W. Chin, A. B. Martin, D. S. King, L. Wang, P. G. Schultz, Addition of a photocrosslinking amino acid to the genetic code of Escherichiacoli. *Proc. Natl. Acad. Sci. U.S.A.* **99**, 11020–11024 (2002). doi:10.1073/pnas.172226299 Medline

35. A. Sharma, M. Mariappan, S. Appathurai, R. S. Hegde, In vitro dissection of protein translocation into the mammalian endoplasmic reticulum. *Methods Mol. Biol.* **619**, 339–363 (2010). doi:10.1007/978-1-60327-412-8_20 Medline

36. Q. Feng, S. Shao, In vitro reconstitution of translational arrest pathways. *Methods* **137**, 20–36 (2018). doi:10.1016/j.ymeth.2017.12.018 Medline

37. K. J. Livak, T. D. Schmittgen, Analysis of relative gene expression data using real-time quantitative PCR and the 2(-Δ Δ C(T)) Method. *Methods* **25**, 402–408 (2001). doi:10.1006/meth.2001.1262 Medline

38. J. Zivanov, T. Nakane, B. O. Forsberg, D. Kimanius, W. J. H. Hagen, E. Lindahl, S. H. W. Scheres, New tools for automated high-resolution cryo-EM structure determination in RELION-3. *eLife* **7**, e42166 (2018). doi:10.7554/eLife.42166 Medline

39. S. Q. Zheng, E. Palovcak, J.-P. Armache, K. A. Verba, Y. Cheng, D. A. Agard, MotionCor2: Anisotropic correction of beam-induced motion for improved cryo-

electron microscopy. *Nat. Methods* **14**, 331–332 (2017). doi:10.1038/nmeth.4193 Medline

40. A. Rohou, N. Grigorieff, CTFFIND4: Fast and accurate defocus estimation from electron micrographs. *J. Struct. Biol.* **192**, 216–221 (2015). doi:10.1016/j.jsb.2015.08.008 Medline

41. S. Shao, J. Murray, A. Brown, J. Taunton, V. Ramakrishnan, R. S. Hegde, Decoding Mammalian Ribosome-mRNA States by Translational GTPase Complexes. *Cell* **167**, 1229–1240.e15 (2016). doi:10.1016/j.cell.2016.10.046 Medline

42. C. J. Adams, A. C. W. Pike, S. Maniam, T. D. Sharpe, A. S. Coutts, S. Knapp, N. B. La Thangue, A. N. Bullock, The p53 cofactor Strap exhibits an unexpected TPR motif and oligonucleotide-binding (OB)-fold structure. *Proc. Natl. Acad. Sci. U.S.A.* **109**, 3778–3783 (2012). doi:10.1073/pnas.1113731109 Medline

43. A. Waterhouse, M. Bertoni, S. Bienert, G. Studer, G. Tauriello, R. Gumienny, F. T. Heer, T. A. P. de Beer, C. Rempfer, L. Bordoli, R. Lepore, T. Schwede, SWISS-MODEL: Homology modelling of protein structures and complexes. *Nucleic Acids Res.* **46**, W296–W303 (2018). doi:10.1093/nar/gky427 Medline

44. A. Brown, F. Long, R. A. Nicholls, J. Toots, P. Emsley, G. Murshudov, Tools for macromolecular model building and refinement into electron cryo-microscopy reconstructions. *Acta Crystallogr. D* **71**, 136–153 (2015). doi:10.1107/S1399004714021683 Medline

45. P. Emsley, B. Lohkamp, W. G. Scott, K. Cowtan, Features and development of Coot. *Acta Crystallogr. D* **66**, 486–501 (2010). doi:10.1107/S0907444910007493 Medline

46. L. Wang, W. Zhang, L. Wang, X. C. Zhang, X. Li, Z. Rao, Crystal structures of NAC domains of human nascent polypeptide-associated complex (NAC) and its αNAC subunit. *Protein Cell* **1**, 406–416 (2010). doi:10.1007/s13238-010-0049-3 Medline

47. V. B. Chen, W. B. Arendall 3rd, J. J. Headd, D. A. Keedy, R. M. Immormino, G. J. Kapral, L. W. Murray, J. S. Richardson, D. C. Richardson, MolProbity: All-atom structure validation for macromolecular crystallography. *Acta Crystallogr. D* **66**, 12–21 (2010). doi:10.1107/S0907444909042073 Medline

48. P. B. Rosenthal, R. Henderson, Optimal determination of particle orientation, absolute hand, and contrast loss in single-particle electron cryomicroscopy. *J. Mol. Biol.* **333**, 721–745 (2003). doi:10.1016/j.jmb.2003.07.013 Medline

49. E. F. Pettersen, T. D. Goddard, C. C. Huang, G. S. Couch, D. M. Greenblatt, E. C. Meng, T. E. Ferrin, UCSF Chimera—A visualization system for exploratory research and analysis. *J. Comput. Chem.* **25**, 1605–1612 (2004). doi:10.1002/jcc.20084 Medline

TTC5 mediates autoregulation of tubulin via mRNA degradation

Zhewang Lin, Ivana Gasic, Viswanathan Chandrasekaran, Niklas Peters, Sichen Shao, Timothy J. Mitchison and Ramanujan S. Hegde

published online November 14, 2019